PROCEEDINGS

OF INTERNATIONAL CONFERENCE ON COMMUNICATIONS, ELECTROMAGNETICS AND MEDICAL APPLICATIONS (CEMA'06)

Organized by:

FACULTY OF COMMUNICATION TECHNIQUE AND TECHNOLOGIES OF TECHNICAL UNIVERSITY OF SOFIA, BULGARIA

NATIONAL TECHNICAL UNIVERSITY OF ATHENS, GREECE, SCHOOL OF ELECTRICAL AND COMPUTER ENGINEERING

Sofia, Bulgaria
19th – 21th October, 2006

KING

Edited by **Dimiter Tz. Dimitrov**

ISBN 10: 954-9518-39-6
ISBN 13: 978-954-9518-39-9

Printed in Bulgaria

D. Dimitrov

Dear Colleagues, Dear Friends,

It's my privilege, as Chairman of the International Scientific Committee to welcome you to take part in the International Conference **Communications, Electromagnetics and Medical Applications (CEMA'06)** to be held this week 19-21th October, 2005 in Sofia.

The Conference is dedicated to all essential aspects of the development of global information and communication technologies and their impact for medicine. The conference is mainly aimed to facilitate the exchange of experience in the field of wireless communications, mobile communications, satellite communications, signal processing techniques, electromagnetics, microwave techniques, electromagnetics in Biology and Medicine, medical imaging techniques (microwave tomographic techniques, x-rays imaging etc.), Telemedicine, computer simulation of electromagnetic field, etc.

The objective of the Conference is to bring together lecturers, researchers and practitioners from different countries, working on the field of communication, electromagnetism and medical applications, computer simulation of electromagnetic field, in order to exchange information and bring new contribution to this important field of engineering design and application in medicine. The Conference will bring you the latest ideas and development of the tools for the above mentioned scientific areas directly from their inventors.

The conference sessions will enable you to experiment with engineering methods for investigation, software for computer simulation and design in communication, electromagnetism and medical applications, presented by participants of the Conference, and to take practical ideas and solutions with you. The Conference will also consolidate the links among the European Universities and also create new ones.

CEMA'06 also give you opportunity to visit Sofia, the Bulgarian capital which is one of the oldest European towns.

Let me take a chance to thank you for your contributions. I would like to thank you personally to the Vice Chairman of Conference, Prof. Frangos for his good ideas and suggestions, for his efforts in the process of preparation of Conference.

This conference can be the first of a series if such is your wish. I hope the next conference in Athens will continue our scientific cooperation.

Dear colleagues , I wish you successful presentations.

Good luck to all participants in the conference.

Dimiter Tz. Dimitrov
Conference Chairman

SCIENTIFIC PROGRAM

Opening ceremony
19th October
11-11h30, room 12134 in 12th building

Lunch
12h-13h30

FIRST SESSION
13h30 – 15h30, room 12134 in 12th building

Chairman: *Prof. A. Bekiarski – Technical University of Sofia, Bulgaria*

1. Ch. G. Moschovitis, E. G. Papkelis, H. T. Anastassiu, K. T. Karakatselos, I. Ch. Ouranos and P. V. Frangos, National Technical University of Athens, Greece, **An application of an enhanced Stationary Phase Method (SPM) approximation for the asymptotic calculation of the scattered electric field from a finite rectangular**
2. V. Karakasiliotis, P. V. Frangos, National Technical University of Athens, Greece, **Decimative Spectrum Estimation Method for High-Resolution Radar Parameter Estimates**
3. S. Ver Hoeye, P. Moreno, D. García, M. Fernández, L. F. Herrán, and F. Las Heras, University of Oviedo, Spain, **Rational synchronization of microwave oscillators for phase-noise improvement**
4. V. Demirev, Technical University of Sofia, Bulgaria, **Broadband satellite SCP-RPSC communications – the new chance for the telemedicine**
5. Petrovska, University Hospital "St.Anna", Medical University of Sofia, Bulgaria, **Advantages and Disadvantages of Magnetotherapy**
6. Dimiter Tz. Dimitrov, Technical University of Sofia, Bulgaria, **An investigation on propagation and absorption of electromagnetic signals through biological media**
7. Dimiter Tz. Dimitrov, Hristo Hristov, Technical University of Sofia, Bulgaria, **Modeling the moving of charges in homogenous magnetic field**

Coffe break
15h30 – 16h

SECOND SESSION

16h – 17h 30, room 12134 in 12th building

Chairman: *Prof. P. Frangos, NTUA, Greece*

1. V. Dumbrava, L. Svilainis, Kaunas University of Technology, Litvania,
   The ultrasonic transducer preamplifier noise performance
2. Song Lixin Gao jie Zhang kaiyu Shi Shengjun, Harbin university of science and technology, P. R. China,
   A computer-aided detection and diagnosis for microcalcifications in digital mammograms
3. Snejana Pleshkova-Bekiarska, Damian Damianov, Technical University of Sofia, Bulgaria,
   CELP Code Book with Index Prediction
4. Alexander Bekiarski, Andrei Andreev, Technical University – Sofia, Bulgaria
   Development of a serial interface for TV monitors adjustment with computer
5. A. Stoilov and V. Hristov, South-West University "Neofit Rilski", Blagoevgrad, Bulgaria,
   FMNSwebDoc – web based system for documentation

Closing Session

17h30 – 18h, room 12134 in 12th building

SOCIAL PROGRAM

Banquet
October, 19th, 19h30

Trip to the town-museum Koprivstica
October, 20th

During the trip a lunch for the conference participants
will be provided as its price is included in the conference fee

REGISTRATION

October, 19th, 9.00h – 18.00h

The conference registration desk will be in the room 12134, 12th building, Faculty of Electrotechnique, Technical University of Sofia. It will be open on Wednesday, October 19th, 9.00h – 18.00h

INTERNATIONAL CONFERENCE

on

Communications, Electromagnetics and Medical Applications

(CEMA'06)

Sofia, Bulgaria
19th – 21th October, 2006

Organized by:

Faculty of Communication Technologies of TU-Sofia, Bulgaria

NATIONAL TECHNICAL UNIVERSITY OF ATHENS, GREECE

SCHOOL OF ELECTRICAL AND COMPUTER ENGINEERING

INTERNATIONAL SCIENTIFIC COMMITTEE

***Honorary Chairman*:** Prof. L. LARENG, President of the European Society of Telemedicine
***Chairman*:** D. C. DIMITROV, Technical University of Sofia, Bulgaria
Vice Chairman: P. FRANGOS, National Technical University of Athens, Greece

MEMBERS:

I. ALIFERIS, University of Nice, France
E.ALTIMIRSKY, Technical University of Sofia, Bulgaria
N. AMPILOVA, University of Perersburg, Russia
R. ARNAUDOV, Technical University of Sofia, Bulgaria
Q. BALZANO, University of Maryland, USA
A. BEKJARSKY, Technical University of Sofia, Bulgaria
J. CATRYSSE, Katholieke Hogenschool Brugge Oostende, Belgium
Ph. CONSTANTINOU, National Technical University of Athens, Greece
J. DAUVIGNAC, University of Nice, France
B. DEKERIS, Kaunas University of Technology, Litvania
V. DEMIREV, Technical University of Sofia, Bulgaria
M. DONTSCHEWA, University of Applied Sciences, Dorbirn, Austria
D. EIDUKAS, Kaunas University of Technology , Litvania
S. Ver HOEYE, University of Oviedo, Spain
M. HOFMANN, University of Ulm, Germany
V. HRISTOV, University of Blagoevgrad, Bulgaria
I. ILIEV, Technical University of Sofia, Bulgaria
R. KRIVICKAS, Kaunas University of Technology, Litvania
G. MALLET, University "Sophia Antipolis", Nice, France
R. De LEO, Universita, Politecnica della Marche, Italy
V. MARINKEV, Medical University of Plovdiv, Bulgaria
M.MARTINS, Instituto Superior Técnico, Lisboa, Portugal
K. NIKITA, National Technical University of Athens, Greece
M. NIKOLOVA, High Naval School, Varna, Bulgaria
M. PASTORINO, University of Genova, Italy
Ch. PICHOT ,University of Nice, France
F. PRATO, University of Western Ontario, Canada
A.SAVOV, Medical University of Sofia, Bulgaria
H-P. SCHADE, Technical University of Ilmenau, Germany
L. SONG, Technical University of Harbin, China
A.USHEVA, University of Boston, USA
N. UZUNOGLU, National Technical University of Athens, Greece
K. VLADIMIROV, Medical University of Sofia, Bulgaria

CONTACT US:
http://www.tu-sofia.bg/fktt/cema06/
http://cema06.atspace.org

GENERAL INFORMATION

Submission of contributions
Hotel reservation

Prof. Dr. Dimiter Dimitrov

Faculty of Communication Technique and Technologies
Technical University of Sofia
8, Kliment Ohridsky str.
1756 Sofia, Bulgaria
Phone: ++359 2 9652278
Fax: ++3592 9741360
E-mail: dcd@tu-sofia.bg

Prof. P. Frangos

National Technical University of Athens
School of Electrical and Computer Engineering
9, Iroon Polytechniou Str. ,
157 73 Zografou, Athens, Greece
Phone: 00 30 210 772 3694
Fax: 00 30 210 772 2281
E-mail: pfrangos@central.ntua.gr

REVIEWERS

N. AMPILOVA, Russia
M. DONTSCHEWA, Austria
F. KLETT, Germany
V. HRISTOV, Bulgaria
G. MALLET, France
R. De LEO, Italy
V. MARINKEV, Bulgaria
M. MARTINS, Portugal
M. NIKOLOVA, Bulgaria
A. SAVOV, Bulgaria
H-P. SCHADE, Germany
L. SONG, China
A. USHEVA, USA
K. VLADIMIROV, Bulgaria
E. BOEMO, Spain
D. DIMITROV, Bulgaria

TABLE OF CONTENTS

AN APPLICATION OF AN ENHANCED STATIONARY PHASE METHOD (SPM) APPROXIMATION FOR THE ASYMPTOTIC CALCULATION OF THE SCATTERED ELECTRIC FIELD FROM A FINITE RECTANGULAR PLATE

Ch. G. Moschovitis, E. G. Papkelis, H. T. Anastassiu, K. T. Karakatselos, I. Ch. Ouranos and P. V. Frangos

National Technical University of Athens, School of Electrical and Computer Engineering,
Division of Information Transmission Systems and Materials Technology,
Radar Systems and Remote Sensing Laboratory,
9 Iroon Polytechniou Str. 15773 Zografou, Athens, Greece
phone: +30210-772-3694 ;fax: +30210-772-2281;
e-mail: pfrangos@central.ntua.gr

Abstract

Propagation in an urban outdoor environment which consists of three dimensional scatterers (walls) is the main goal of our research. Provided that both transmitter and receiver are located below rooftop level, this scenario pertains to propagation circumstances related to modern high frequency communication wireless networks. Such environment could be modeled through the prerequisite problem of an electromagnetic (EM) wave which is assumed to be incident on a perfectly conducting rectangular plate of finite dimensions.

Our contribution to the problem is a simulation application, which is based on an enhanced Stationary Phase Method asymptotic approximation for the calculation of the scattered electric field from a finite rectangular plate.

Our principal result is an SPM formula which produces thorough results analytically proven to correspond to a plane wave. The novel, important feature of our approach is the inclusion of the edge contribution to the resulting asymptotic expressions using – simple to implement, yet complicated in terms of results - improved edge contribution forms, which have not been documented in the literature for the case of a double integral.

Simulation results are compared to results obtained with standard numerical integration, though SPM divulged here is incomparably faster.

1. Introduction

Let us consider the observation point Rx(x,y,z) in a propagation problem layout of an electromagnetic (EM) wave with wavevector k_i, which is assumed to be incident on a perfectly conducting rectangular plate of finite dimensions.

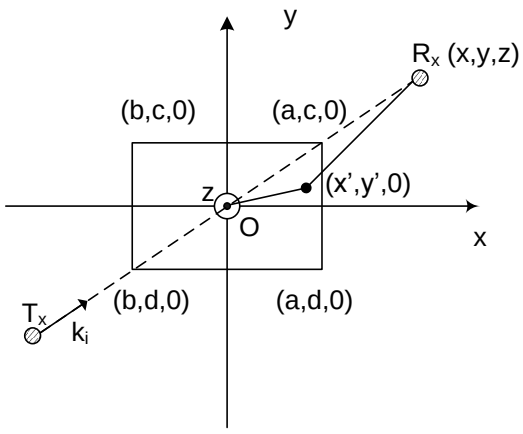

Figure 1. 3D geometry xy plane projection

This three dimensional scatterer is the necessary prerequisite in order to model propagation in an urban outdoor environment, which consists of three dimensional walls and obstacles that often pertain to modern high frequency

communication wireless networks, such as GSM, UMTS, Wi-Fi and Wi-Max technologies. Should the rectangular plate lie on the xy plane, two different approaches are distinguished according to the polarization of the incident field (TE + TM polarization).

2. Vector Potential $\vec{A}$ and Scattered Electric Field $\vec{E}$

According to P.O theory, the current density is equal to Eq. 1:

$$\vec{J}_s^{P.O} = 2 \cdot n \times \vec{H}_i \Big|_{\substack{z=0 \\ y=y'}} = \hat{x} \cdot 2 \cdot \frac{E_0}{\eta} \cdot \cos \vartheta_i \cdot \cdot \exp\left[- j \cdot k \cdot y' \cdot \sin \vartheta_i \right] \quad (1)$$

By utilising the three dimensional Green function (Eq. 2):

$$G(r,r') = \frac{\exp\left(-j \cdot k \cdot |r - r'|\right)}{4\pi \cdot |r - r'|} \quad (2)$$

the vector potential $\vec{A}$ at the observation point $R_x(x,y,z)$ is given by Eq. 3:

$$\underline{A}(x,y,z) = \mu_0 \cdot \int_{y'=d}^{c} \int_{x'=b}^{a} \left[\vec{J}_s^{P.O}(x',y') \cdot G(r,r') \right] \cdot dx'dy' \quad (3)$$

Substitution of total current density yields the potential vector expression (Eq. 4) for both TE and TM polarization:

$$\underline{A}(x,y,z) = \frac{-\mu_0}{2\pi \cdot \eta} \cdot [\hat{x} \cdot (E_{0\theta} \cdot \cos\phi_i - \mathrm{E}_{0\phi} \cdot \cos\theta_i \cdot \sin\phi_i) + + \hat{y} \cdot (E_{0\theta} \cdot \sin\phi_i + E_{0\phi} \cdot \cos\theta_i \cdot \cos\phi_i)] \cdot \int_{y'=d}^{c} \int_{x'=b}^{a} \frac{\exp\left\{ j \cdot k \left[\begin{array}{l} (x' \cdot K + y' \cdot L) - \\ - \sqrt{(x-x')^2 + (y-y')^2 + z^2} \end{array} \right] \right\}}{\sqrt{(x-x')^2 + (y-y')^2 + z^2}} dx'\,dy' \quad (4)$$

since it is easily obtained from Fig. 1 that

$$|\underline{r} - \underline{r'}| = \sqrt{(x-x')^2 + (y-y')^2 + z^2} \quad (5)$$

and K, L constants which depend on the incident angles θ_i and φ_i satisfying Eqs. 6-7:

$$K = \sin\theta_i \cdot \cos\phi_i \quad (6)$$

$$L = \sin\theta_i \cdot \sin\phi_i \quad (7)$$

Finally the scattered electric field is calculated from the formula:

$$\underline{E}_s(x,y,z) = -j \cdot \omega \cdot \underline{A} - j \cdot \frac{\omega}{k^2} \cdot grad\left(div(\underline{A})\right) \quad (8)$$

3. SPM approximations

Operating at the frequency of 1GHz or higher, scatterers that appear in the above networks are considered to be electrically large, and current density may be calculated with good accuracy using the physical optics (P.O.) approximation. Modifying appropriately Eq. 4 we can apply SPM approximations which result in calculating the vector potential and eventually the total scattered electric field at the observation point $R_x(x,y,z)$. The functions we use are derived in Eqs. 9-10:

$$F(x',y') = \frac{1}{\sqrt{(x-x')^2 + (y-y')^2 + z^2}} \quad (9)$$

$$f(x',y') = x'K + y'L - \sqrt{(x-x')^2 + (y-y')^2 + z^2} \quad (10)$$

The novel, important feature of our approach is the inclusion of the edges contribution to the resulting asymptotic expressions, which has not been documented in the literature for a double integral. In some cases [1] a literature approach for the solution of the above problem cannot be applied. This solution is achieved by inserting a rotation of the three dimensional system using spherical coordinates variables, resulting in rather complicated formulas which are not easy to neither handle,

nor implement or utilize in a modern propagation simulation tool. Additionally, the results of this rotation, due to the extreme complexity of the analytical values they include, are unable to produce an effective series of fast and adequate results.

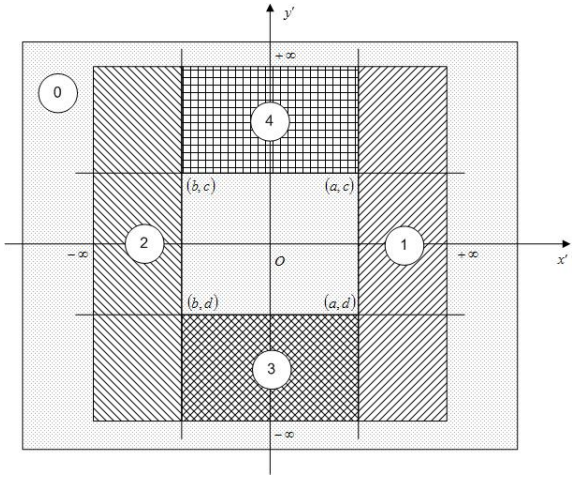

Figure 2. SPM approach

Our approach is illustrated in Fig. 4. According to this procedure, the initial integral, which is to be computed, is extended to infinite for both x' and y' variables. This extension primarily enables us to utilize the standard SPM formulas, documented for an infinite integral [2]. Since the plate is finite, additional correction terms should be included in the final SPM result. Those terms are obtained by subtracting the remaining areas around the finite plate. For those terms, the results are computed by utilizing a combination of SPM and edge contribution side formulas, thoroughly documented but only for the case of a single integral. By applying such calculations twice, we present here new functions on which we re-apply SPM approximations, and finally result in avoiding the complicated variable rotation and making the solution applicable. Using this technique we are also able to present thorough analytical results, which for the case of the double integral are really complicated. Eqs. 11-37 present the method explained above:

$$I(k)=\int_{y'=d}^{c}\int_{x'=b}^{a}F(x',y')\cdot e^{j\cdot k\cdot f(x',y')}dx'\cdot dy'=$$
$$\int_{-\infty-\infty}^{+\infty+\infty}F(x',y')\cdot e^{j\cdot k\cdot f(x',y')}dx'\cdot dy'-\int_{-\infty x'=a}^{+\infty+\infty}F(x',y')\cdot e^{j\cdot k\cdot f(x',y')}dx'\cdot dy'-$$
$$-\int_{-\infty-\infty}^{+\infty x'=b}F(x',y')\cdot e^{j\cdot k\cdot f(x',y')}dx'\cdot dy'-\int_{-\infty x'=b}^{y'=d\ a}F(x',y')\cdot e^{j\cdot k\cdot f(x',y')}dx'\cdot dy'-$$
$$-\int_{y'=c\ x'=b}^{+\infty\ a}F(x',y')\cdot e^{j\cdot k\cdot f(x',y')}dx'\cdot dy'\Rightarrow$$
$$I(k)=I[0]-I[1]-I[2]-I[3]-I[4] \tag{11}$$

$$I[0]=\int_{-\infty-\infty}^{+\infty+\infty}F(x',y')\cdot\exp\left(j\cdot k\cdot f(x',y')\right)\cdot dx'\cdot dy'=$$
$$=F(x_s,y_s)\cdot\frac{j\cdot 2\cdot\pi\cdot\delta}{k\cdot\sqrt{\left|4A\cdot B-C^2\right|}}\cdot\cdot\exp\left(j\cdot k\cdot f(x_s,y_s)\right) \tag{12}$$

where

k: real number, relatively high.

x_s, y_s: Stationary points of f, i.e. the points for which both the partial derivatives of f in respect to x' and y' variables are zero.

$$\left.\frac{\partial f}{\partial x'}\right|_{\substack{x=x_s\\y=y_s}}\equiv f'_{x'}(x_s,y_s)=0 \tag{13}$$

$$\left.\frac{\partial f}{\partial y'}\right|_{\substack{x=x_s\\y=y_s}}\equiv f'_{y'}(x_s,y_s)=0 \tag{14}$$

f(x,y): Slow varying, real, non-linear function, independent of k.

F(x,y): Non-linear function, may be complex, but should also be independent of k.

a, b, c, d: Limits of double integral. The information of the limits is included in the location of stationary points x_s, y_s.

A, B, C: Constants related to the derivatives of function f which are calculated from Eqs. 15-17:

$$A=\frac{1}{2}\cdot f''_{xx}(x_s,y_s) \tag{15}$$

$$B=\frac{1}{2}\cdot f''_{yy}(x_s,y_s) \tag{16}$$

$$C=f''_{xy}(x_s,y_s) \tag{17}$$

δ: Value of δ is defined from the relative values of A, B, C constants:

$$\delta = \begin{cases} +1 & , \quad 4A \cdot B > C^2, A > 0 \\ -1 & , \quad 4A \cdot B > C^2, A < 0 \\ -j & , \quad 4A \cdot B < C^2 \end{cases} \qquad (18)$$

$$I[1] = \int_{-\infty x'=a}^{+\infty \; +\infty} F(x', y') \cdot e^{j \cdot k \cdot f(x', y')} dx' \cdot dy' =$$

$$= \sqrt{\frac{2 \cdot \pi}{k \cdot \left| \frac{\partial^2 f'_{(02)}}{\partial y'^2} \right|_{y'=y_{02}}}} \cdot F'_{(02)}(y_{02}) \cdot$$

$$\cdot \exp\left(j \left[k \cdot f'_{(02)}(y_{02}) + \frac{\pi}{4} \cdot \operatorname{sgn}\left\{ \left. \frac{\partial^2 f'_{(02)}}{\partial y'^2} \right|_{y'=y_{02}} \right\} \right] \right) \qquad (19)$$

$$I[2] = \int_{-\infty \; -\infty}^{+\infty x'=b} F(x', y') \cdot e^{j \cdot k \cdot f(x', y')} dx' \cdot dy' =$$

$$= \sqrt{\frac{2 \cdot \pi}{k \cdot \left| \frac{\partial^2 f'_{(03)}}{\partial y'^2} \right|_{y'=y_{03}}}} \cdot F'_{(03)}(y_{03}) \cdot$$

$$\cdot \exp\left(j \left[k \cdot f'_{(03)}(y_{03}) + \frac{\pi}{4} \cdot \operatorname{sgn}\left\{ \left. \frac{\partial^2 f'_{(03)}}{\partial y'^2} \right|_{y'=y_{03}} \right\} \right] \right) \qquad (20)$$

$$I[3] = \int_{-\infty \; x'=b}^{y'=d \; a} F(x', y') \cdot e^{j \cdot k \cdot f(x', y')} dx' \cdot dy' =$$

$$= \int_{-\infty}^{y'=d} (I'_0 - I'_a - I'_b) \cdot dy' =$$

$$= I[3.1] - I[3.2] - I[3.3] \qquad (21)$$

$$I[3.1] = \int_{-\infty}^{y'=d} I_o \cdot dy' = \frac{1}{jk} \cdot \frac{F'_{(01)}(d)}{\left. \frac{\partial f'_{(01)}}{\partial y'} \right|_{y'=d}} \cdot \exp\left\{ jk \cdot f'_{(01)}(d) \right\} \qquad (22)$$

$$I[3.2] = \int_{-\infty}^{y'=d} I_a \cdot dy' = \frac{1}{jk} \cdot \frac{F'_{(02)}(d)}{\left. \frac{\partial f'_{(02)}}{\partial y'} \right|_{y'=d}} \cdot \exp\left\{ jk \cdot f'_{(02)}(d) \right\} \qquad (23)$$

$$I[3.3] = \int_{-\infty}^{y'=d} I'_b \cdot dy' = \frac{1}{jk} \cdot \frac{F'_{(03)}(d)}{\left. \frac{\partial f'_{(03)}}{\partial y'} \right|_{y'=d}} \cdot \exp\left\{ jk \cdot f'_{(03)}(d) \right\} \qquad (24)$$

$$I[4] = \int_{y'=c}^{+\infty \; a} \int_{x'=b} F(x', y') \cdot e^{j \cdot k \cdot f(x', y')} dx' \cdot dy' =$$

$$= \int_{y'=c}^{+\infty} (I'_o - I'_a - I'_b) \cdot dy' = \qquad (25)$$

$$= I[4.1] - I[4.2] - I[4.3]$$

$$I[4.1] = \int_{y'=c}^{+\infty} I'_o \cdot dy' = -\frac{1}{jk} \cdot \frac{F'_{(01)}(c)}{\left. \frac{\partial f'_{(01)}}{\partial y'} \right|_{y'=c}} \cdot \exp\left\{ jk \cdot f'_{(01)}(c) \right\} \qquad (26)$$

$$I[4.2] = \int_{y'=c}^{+\infty} I'_a \cdot dy' = -\frac{1}{jk} \cdot \frac{F'_{(02)}(c)}{\left. \frac{\partial f'_{(02)}}{\partial y'} \right|_{y'=c}} \cdot \exp\left\{ jk \cdot f'_{(02)}(c) \right\} \qquad (27)$$

$$I[4.3] = \int_{y'=c}^{+\infty} I'_b \cdot dy' = -\frac{1}{jk} \cdot \frac{F'_{(03)}(c)}{\left. \frac{\partial f'_{(03)}}{\partial y'} \right|_{y'=c}} \cdot \exp\left\{ jk \cdot f'_{(03)}(c) \right\} \qquad (28)$$

Final results are obtained when substituting functions included in Eqs. 19-28 with the corresponding expressions using Eqs. 29-34, listed below:

$$F'_{(01)}(y') = \sqrt{\frac{2\pi}{k \left| \frac{\partial^2 f}{\partial x'^2} \right|_{x'=x_o, y'=y'}}} F(x_o, y') \cdot$$

$$\cdot \exp\left(j \cdot \frac{\pi}{4} \operatorname{sgn}\left\{ \left. \frac{\partial^2 f}{\partial x'^2} \right|_{x'=x_o, y'=y'} \right\} \right) \qquad (29)$$

$$f'_{(01)}(y') = f(x_o, y') \qquad (30)$$

$$F'_{(02)}(y') = -\frac{1}{jk} \cdot \frac{F(a, y')}{\left. \frac{\partial f}{\partial x'} \right|_{x'=a, y'=y'}} \qquad (31)$$

$$f'_{(02)}(y') = f(a, y') \qquad (32)$$

$$F'_{(03)}(y') = \frac{1}{jk} \cdot \frac{F(b, y')}{\left. \frac{\partial f}{\partial x'} \right|_{x'=b, y'=y'}} \qquad (33)$$

$$f'_{(03)}(y') = f(b, y') \qquad (34)$$

Equations I[1], I[2], I[3.1] and I[4.1] include the stationary points x_0 and y_{02}, y_{03} respectively. Since these integral terms refer to modified stationary points, as shown in Eqs. 35-37 below, their contribution will be included in the final result, only if these points are located between [c,d] and [b,a] respectively. In any other case, the contribution of these integral terms is zero.

$$\left.\frac{\partial f(x',y')}{\partial x'}\right|_{x'=x_o,y'=y'} = 0 \qquad (35)$$

$$\left.\frac{\partial f'_{(02)}(y')}{\partial y'}\right|_{y'=y_{02}} = 0 \qquad (36)$$

$$\left.\frac{\partial f'_{(03)}(y')}{\partial y'}\right|_{y'=y_{03}} = 0 \qquad (37)$$

4. Simulation Results

Furthermore, in order to check the accuracy of our asymptotic calculations, standard (e.g. Gaussian) numerical integration was used to compare the results. Due to the complexity of the functions on which SPM is applied, the calculations were carried out using MATLAB's symbolic toolbox. A simulating application was also developed for the asymptotic SPM calculations. Results derived from MATLAB calculations constitute an aggregation of complicated formulas. Assuming an appropriate set of simulation parameters, the total electric field was calculated for distances in the Far Field, Fresnel Region and Near Field area. We compared SPM method and numerical integration for the frequency of 1GHz and for rectangular plates with side length equal to 20λ, 40λ, 60λ and 80λ. Both the elevation and azimuth angles of incidence were assumed equal to 45 degrees.

Comparison charts in Figs. 3 – 8 above indicate reasonable convergence between the asymptotic results of the SPM method, drawn with solid line, and the numerical results of standard integration, drawn with dashed line.

4.1. Small Scatterer

In Figs. 3 – 5, numerical results are shown for a rectangular plate of side dimension 20λ in the Near Field area (r=25m), the Fresnel area (r=100m) and the Far Field area (r=300m).

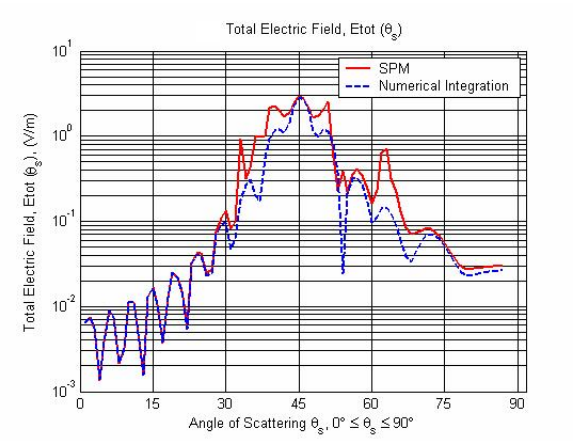

Figure 3. 20λ plate side, Near Field area

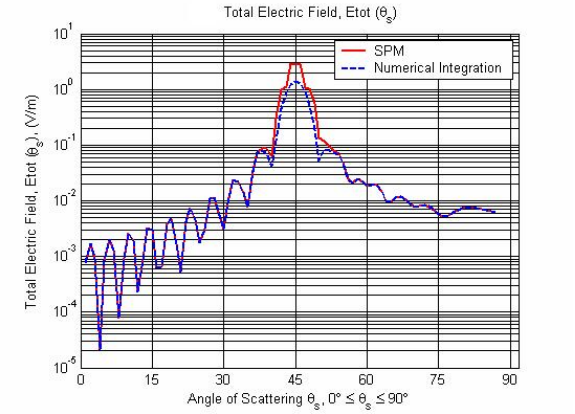

Figure 4. 20λ plate side, Fresnel area

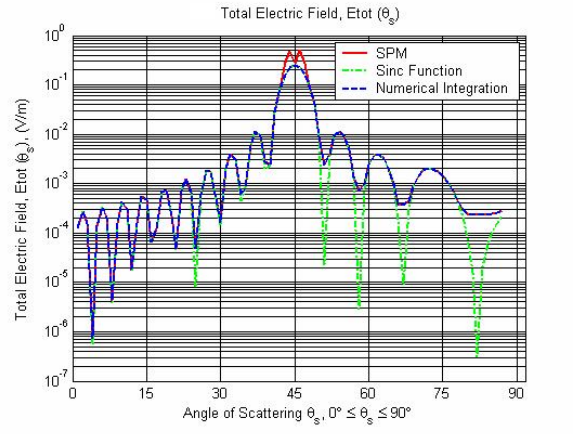

Figure 5. 20λ plate side, Far Field area

4.2. Large Scatterer

In Figs. 6 – 8, we provide results for the case of a larger scatterer of side dimension 80λ in the Near Field area

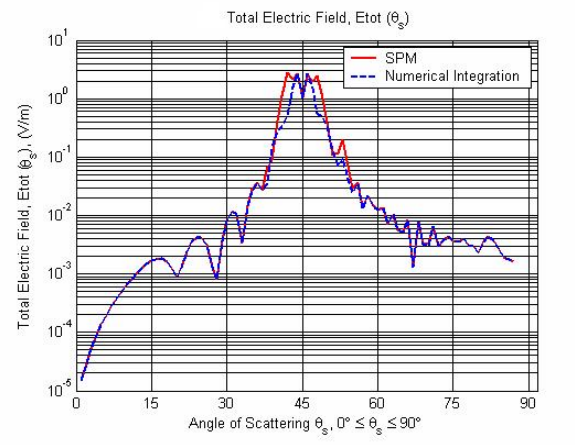

Figure 6. 80λ plate side, Near Field area

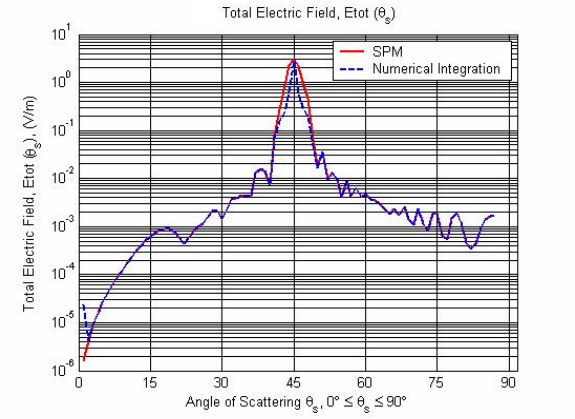

Figure 7. 80λ plate side, Fresnel area

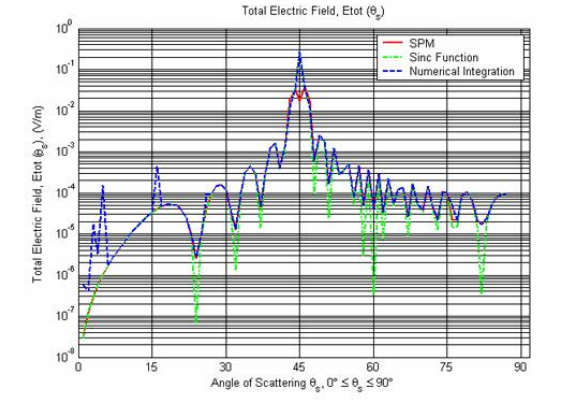

Figure 8. 80λ plate side, Far Field area

(r=100m), the Fresnel area (r=1000m) and the Far Field area (r=4500m).

These numerical results show satisfactory agreement between the two methods of computation for both cases of 20λ plate side and 80λ plate side scatterers. Deviations of the main lobe, which occur in the far field area only for both 20λ and 80λ plate side scatterers, are justified by the behaviour of Eqs. 22-24 and Eqs. 25-27.

5. Conclusion

Even though rather complicated mathematical formulas are involved in the proposed SPM method, it is very important that this technique is much faster than the numerical integration. Namely, SPM in this case is about 40 times faster. We can very easily understand how important this is for the numerical implementation of a simulated propagation problem in an urban outdoor environment, in which case many scatterers (walls) and multiple reflection phenomena are present. Furthermore, by increasing the dimensions of the scatterer, we are effectively increasing the frequency, thus reducing the error. The SPM method presented here appears to be very attractive for the calculation of vector potential $\vec{A}$ and electric field $\vec{E}$ in various radio propagation simulation tools.

Future development includes amelioration of the behaviour of the main lobe by reducing the errors using additional factorial integration.

References

[1] Graeme L. James, Geometrical Theory Of Diffraction for Electromagnetic Waves, UK, IEE 1976, pp. 30-42.

[2] C. A. Balanis, "Antenna Theory: Analysis and Design", John Wiley & Sons, NY, 1996, pp. 922-926.

[3] C. A. Balanis, "Advanced Engineering Electromagnetics", John Wiley & Sons, NY, 1989, pp. 586 -594.

[4] David C. Jenn, Radar and Laser Cross Section Engineering, American Institute of Aeronautics and Astronautics, Inc. Washington, 1995, pp. 29-33.

DECIMATIVE SPECTRUM ESTIMATION METHOD FOR HIGH-RESOLUTION RADAR PARAMETER ESTIMATES

A. V. Karakasiliotis, P. V. Frangos

National Technical University of Athens, School of Electrical and Computer Engineering,
Division of Information Transmission Systems and Materials Technology,
Radar Systems and Remote Sensing Laboratory,
9 Iroon Polytechniou Street, 15773 Zografou, Athens, Greece
phone: +30210-772-3694 ;fax: +30210-772-2281;
e-mail: taskarak@mail.ntua.gr, pfrangos@central.ntua.gr

Abstract

Scattering center extraction for radar targets is strongly related to high-resolution parameter estimation.

In this paper, we propose the use of a decimative spectrum estimation method (DESED) for the estimation of the parameters of a synthetic radar signal. DESED is compared to two variants of the widely applied root-MUSIC algorithm, in terms of range and amplitude estimation errors.

The proposed method outperforms root-MUSIC with modified spatial smoothing pre-processing, for both well-separated and closely spaced point scatterers. Additionally, it appears to be slightly more accurate than root-MUSIC with decimation, especially for low signal-to-noise ratio and in the case of well-separated point scatterers.

1. Introduction

Parameter estimation is a fundamental field of signal processing. Two main approaches are followed: Bayes estimation which is based on a priori knowledge about the examined signal (probability distribution functions of parameters), and maximum likelihood (ML) estimation which maximizes a likelihood function that depends on signal parameters. Algorithms based on singular value decomposition (SVD) have been proposed to solve the parameter estimation problem [1]. With the recent advance of digital signal processors (DSP) and personal computers, moderately sized SVD analysis (square matrix order of 50-70) has become feasible and computationally efficient software implementations are available. For this reason, parameter estimation methods that embody SVD appear to be appealing, resulting in estimation accuracy at the cost of additional computational burden.

High-resolution radar imaging is performed with the use of spectrum estimation methods [2], [3]. Parametric methods are of special interest, since they employ a parametric model to accurately describe the signal segment under spectral analysis. A parameter vector has to be estimated before the computation of the signal's spectral content. Thus, parameter estimation is highly related to radar imaging, and is a primary step of the whole process.

Decimative spectrum estimation constitutes a very interesting field of signal processing research [4], [5], [6], compared to the classical methods that were proposed a few decades ago. Decimation improves resolution capability of a frequency estimation method. In [5], two superresolution subspace methods, namely MUSIC and ESPRIT, are shown to provide more accurate frequency estimates when data decimation is applied. Furthermore, in [4] it is pointed out that these methods impose

a constraint on the model order with respect to the decimation factor, resulting in reduced efficiency in case of an overdetermined model.

In this paper, we propose the use of a decimative spectrum estimation method, namely DESED [4], for estimating the parameters of a radar signal model, which is based on the geometrical theory of diffraction (GTD). The adopted model has been proved to perform accurate modeling of the backscattered field for a wide range of scatterers [7]. Therefore, using GTD-based model for the description of the received frequency-domain samples of a stepped frequency (SF) radar waveform is reasonable.

DESED method makes use of decimation and SVD, exploits all data available, and does not impose any constraint on the decimation factor and the model order. Frequencies, dam-ping factors and complex amplitudes of the damped exponential (DE) signal model are estimated by DESED. In case of radar scattering data, radial locations, geometry parameters and scattering amplitudes can be respe-ctively derived through mathematical expressions relating DE and GTD models.

The remainder of the paper is organized as follows. Section 2 briefly delineates the GTD-based parametric model for radar scattering, while Section 3 provides the theoretical background of the DESED method. Section 4 presents the simulation results obtained by DESED method and two superresolution techniques, with respect to the estimation of the radar signal parameters. Namely two variants of the root-MUSIC algorithm are compared to DESED method, and useful conclusions are drawn in Section 5.

2. Scattering Model

Radar targets can be adequately characterized by a small number of scattering centers, in the high-frequency limit. The GTD-based model [7], which is used in the present study, provides a parametric description of the measured scattering behavior of a radar target. Its main advantage is that it embodies a parameter that characterizes the geometry of each scattering center. Its accuracy is attributed to its close relation with the physics of electromagnetic scattering. As stated in [7], the GTD-based model describes the frequency dependence of the scattering data more accurately than the DE model. Especially for large relative radar bandwidths, the DE model fails to satisfactorily represent canonical scattering mechanisms and results in worse scattering center resolution than the GTD model.

The GTD model equation for the backscattered field of a perfectly conducting target is:

$$E(f) = \sum_{i=1}^{M} A_i \left(\frac{f}{f_c} \right)^{\alpha_i} e^{-j4\pi f r_i / c} \qquad (1)$$

where f denotes the radar frequency, M is the number of scattering centers, A_i, α_i and r_i symbolize the scattering amplitude, the geometry parameter and the range position of the *i*th scattering center, f_c is the center frequency, and c is the speed of light. Table 1 summarizes the geometry parameters for a number of canonical scattering geometries.

In case of SF waveform, the N frequencies spanning the utilized radar bandwidth are given by:

$$f_n = f_c + n \cdot \Delta f, \quad n = -\frac{(N-1)}{2}, \ldots, \frac{(N-1)}{2} \qquad (2)$$

where N is assumed to be odd in order to provide symmetry around the center frequency, and Δf is the chosen frequency step.

The GTD model can precisely describe various scattering mechanisms. In [7], edge and corner diffractions, as well as reflection mechanisms from three canonical surfaces (sphere, cylinder at broadside and flat plate), are shown to be in accordance to the GTD model. Thus, it stands to reason that a radar target can be considered as a collection of several different scattering geometries, as those cited in Table 1.

Table 1. Geometry parameters for canonical scattering geometries

Example scattering geometries	Geometry parameter value
corner diffraction	– 1
edge diffraction	– ½
ideal point scatterer; doubly curved surface reflection; straight edge specular	0
singly curved surface reflection	½
flat plate at broadside; dihedral	1

3. Proposed Method

Decimative spectrum estimation by a factor of D (DESED) has been introduced in [4]. Frequencies and damping factors are estimated both in least squares (LS) and total least squares (TLS) sense. Amplitude estimation is accomplished in LS sense, by substituting frequency and damping factor estimates in the model equation for the noiseless signal.

DESED assumes that the spectrally analyzed signal is represented by the generalized sinusoidal (also known as damped exponential) model:

$$s(n) = \sum_{i=1}^{p} \left(a_i \, e^{j\phi_i} \right) \cdot e^{(-d_i + j2\pi f_i)n}$$

$$= \sum_{i=1}^{p} g_i \cdot z_i^n \;, \quad n = 0, 1, \ldots, N-1 \tag{3}$$

where p is the model order, a_i, ϕ_i, d_i and f_i denote the amplitude, phase, damping factor and frequency of the *i*th sinusoid, and N is the number of data samples. Equation (3) describes the noiseless signal under spectral analysis. Nonetheless, noisy data measurements are encountered in practical applications, and the noise is usually assumed to be additive white Gaussian (AWGN).

The algorithmic steps of the LS-DESED method are the following:

Step 1: Computation of the Hankel matrix S from the N data points of the examined signal $s(n)$, using equation (3). The Hankel matrix is formulated as follows:

$$S = \begin{pmatrix} s(0) & s(1) & \ldots & s(M-1) \\ \vdots & \vdots & \ddots & \vdots \\ s(L-1) & s(L) & \cdots & s(N-1) \end{pmatrix} \tag{4}$$

Step 2: Derivation of the decimated versions of the Hankel matrix, $S_{\downarrow D}$ by deleting the top D rows of S, and $S_{\uparrow D}$ by deleting the bottom D rows of S.

Step 3: SVD decomposition of matrix $S_{\uparrow D}$, resulting in $S_{\uparrow D} = U_{\uparrow D} \Sigma_{\uparrow D} V_{\uparrow D}^H$, and truncation to order p, by retaining only the p largest singular values in matrix $\Sigma_{\uparrow D}$ and only the first p columns of matrices $U_{\uparrow D}$ and $V_{\uparrow D}$. The resulting matrix is given by:

$$S_{\uparrow D}^{trunc} = U_{\uparrow D}^{trunc} \, \Sigma_{\uparrow D}^{trunc} \left(V_{\uparrow D}^{trunc} \right)^H \tag{5}$$

Step 4: Computation of the truncated SVD solution of equation $X \cdot S_{\uparrow D} = S_{\downarrow D}$ in LS

sense, where X is an $(L-D)$-order matrix:

$$X = S_{\downarrow D} \cdot \left(S_{\uparrow D}^{trunc} \right)^{\dagger} \qquad (6)$$

where $A^{\dagger}$ denotes the pseudo-inverse of a matrix A.

Step 5: Estimation of frequencies f_i and damping factors d_i ($i = 1, \ldots, p$) through the p largest eigenvalues of matrix X, which are proven in [4] to be equal to the decimated signal pole estimates z_i^D. Note from equation (3) that the signal poles are given by $z_i = e^{(-d_i + j2\pi f_i)}$.

Step 6: Estimation of amplitudes a_i and phases ϕ_i ($i = 1, \ldots, p$) by finding a LS solution to equation (3), with z_i replaced by the respective estimates of the previous step and $s(n)$ being the noisy measured data.

The only constraints set by DESED concern the dimensions of the Hankel matrix and its decimated versions. These are:

$$p \le L - D \le M \qquad (7)$$

$$L + M - 1 \equiv N \qquad (8)$$

It worths mentioning that the best results of DESED come from decimated Hankel matrices as square as possible ($L - D \approx M$).

4. Simulation Results

In our simulations, we assume that the radar target consists of ideal point scatterers, and for this reason we simulate the GTD model with zero-valued geometry parameters.

LS-DESED method and two variants of the root-MUSIC algorithm, with modified spatial smoothing pre-processing (MSSP) [8], and with decimation [5], have been tested for two simulation scenarios. The first simulation scenario involves well-separated point scatterers (five distinct radial positions), whereas the second scenario includes two scatterers separated in range by $\frac{1}{3}$ of the Fourier bin δr. All scattering amplitudes are set to unity.

Choosing the radar bandwidth $B = 400\,MHz$ and the center frequency $f_c = 9\,GHz$, the scatterers' separation is calculated: $\Delta r = \left(c / 2B \right) / 3 = 0.125\,m$. The relative radar bandwidth takes the value of $\gamma = B / f_c \approx 0.044$, which is small enough to justify the assumption that the DE model approximates the GTD model. The radar frequency step is set to $\Delta f = 2\,MHz$, resulting in a total of $N = 201$ frequency-domain data samples.

In view of equations (1) and (3), taking into account the assumption of small relative bandwidth, we can easily deduce the mathematical relationship between the frequency estimates of the DE model and the range estimates of the GTD model:

$$r_i = -\frac{c\, f_i}{2\Delta f} \qquad (9)$$

Average RMS values of the range and amplitude estimation errors have been derived for the LS-DESED and the two root-MUSIC variants, for a total of 100 Monte-Carlo trials. The data snapshot length for the root-MUSIC techniques is selected to be $m = 40$, providing a satisfactory tradeoff between frequency resolution and accuracy in the covariance matrix estimate. Decimation factor D takes two values, 2 and 3, for the two techniques that use decimation.

Figs. 1 and 2 graphically depict simulation results in the case of well-separated scatterers, for signal-to-noise ratio (SNR) ranging from 5 to 40 dB. For the second simulation scenario, we present the respective graphs for range estimates in Fig. 3. Table 2 displays the average range estimation errors for the forth and the fifth point scatterer, which are separated by $\delta r/3$. Only the two decimative methods are compared, for decimation factor of 3.

As we can observe from Figs. 1 and 3, the DESED method outperforms root-MUSIC with MSSP, in terms of range estimates. In the case of closely spaced scatterers, the proposed method breaks down at an average SNR value of 15 dB, whereas the root-MUSIC with MSSP is already deteriorated at 25 dB. All three figures indicate that the two decimative methods exhibit similar performance in terms of range and amplitude estimates. DESED appears to be slightly better than root-MUSIC with decimation, and both techniques provide increased resolution compared to the root-MUSIC with MSSP. Furthermore, it is obvious from these results that negligible estimation accuracy can be gained by increasing the decimation factor from 2 to 3. This can be attributed to the relatively short data length.

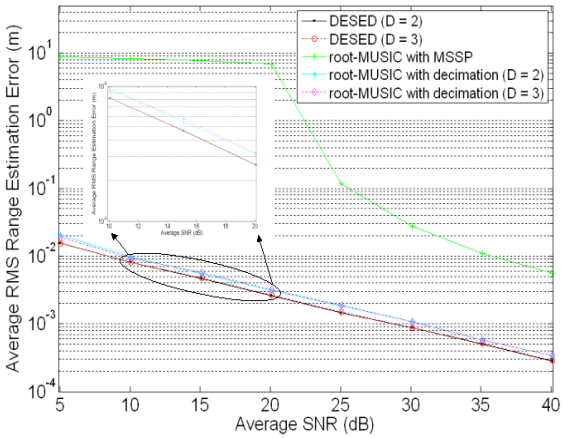

Figure 1. Average RMS range estimation error versus average SNR for well-separated point scatterers

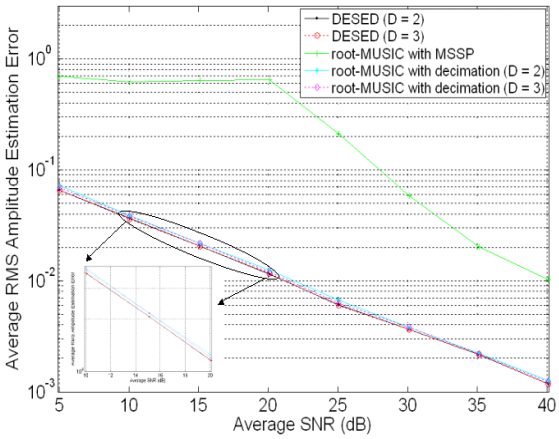

Figure 2. Average RMS amplitude estimation error versus average SNR for well-separated point scatterers

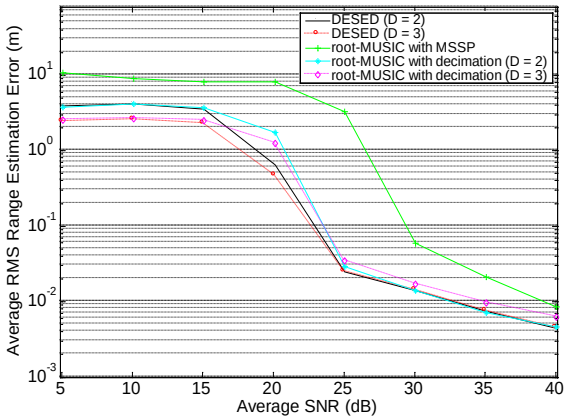

Figure 3. Average RMS range estimation error versus average SNR for closely spaced point scatterers

Table 2. average range estimation errors for two closely spaced point scatterers

SNR (dB)	Average range estimation error (m)			
	Forth scatterer		Fifth scatterer	
	DESED (D = 3)	root-MUSIC (D = 3)	DESED (D = 3)	root-MUSIC (D = 3)
5	1.0930	1.0468	1.6454	1.7395
10	1.1503	1.0103	1.5067	1.9683
15	0.9613	0.9118	1.6680	1.8995
20	0.2492	0.7518	0.3966	0.8590
25	0.0331	0.0601	0.0388	0.0393
30	0.0187	0.0232	0.0210	0.0260
35	0.0107	0.0114	0.0105	0.0137
40	0.0065	0.0088	0.0063	0.0087

5. Conclusions

In this paper, we have proposed the use of a decimative spectrum estimation method, named DESED, for the estimation of the parameters of a synthetic radar signal. The proposed method is much more accurate than the classical root-MUSIC algorithm, in terms of range and amplitude estimates. Simulation results for both well-separated and closely spaced point scatterers reveal slightly better performance than the root-MUSIC method that uses decimation.

Acknowledgment

The authors would like to thank Prof. G. Carayannis, Dr. I. Dologlou, Dr. M. Dendrinos, S. Karabetsos, and P. Tsiakoulis, of the Institute for Speech and Language Processing, Athens, Greece, for the useful discussions regarding the preparation of this paper.

References

[1] A-J. van der Veen, E. F. Deprettere, and A. L. Swindlehurst, "Subspace-based signal analysis using singular value decomposition," *Proc. IEEE*, vol. 81 (9), pp. 1277–1308, Sept. 1993.

[2] M. Cátedra, J. Pérez, F. Fernández, and I. Montiel, "A comparison between super-resolution methods for ISAR," *RTO Meeting Proceedings 40: High Resolution Radar Techniques*, Nov. 1999.

[3] A. V. Karakasiliotis, and P. V. Frangos, "Comparison of several spectral estimation methods for application to ISAR imaging," *Proceedings of RTO SET 080 Panel Symposium*, Oslo, Norway, pp. 1058–1067, 11-13 Oct. 2004.

[4] S-E. Fotinea, I. Dologlou, and G. Carayannis, "A new decimative spectral estimation method with unconstrained model order and decimation factor," in *Total Least Squares and Errors-in-Variables Modeling: Analysis, Algorithms and Applications*, 1st ed., Kluwer editions, 2002, pp. 317–326.

[5] P. Stoica, and A. Nordsjo, "Subspace-based frequency estimation in the presence of moving-average noise using decimation," *Signal Processing*, vol. 63 (3), pp. 211–220, 1997.

[6] B. Halder, and T. Kailath, "Efficient estimation of closely spaced sinusoidal frequencies using subspace-based methods," *IEEE Signal Proc. Letters*, vol. 4 (2), pp. 49–51, Feb. 1997.

[7] L. C. Potter, D-M. Chiang, R. Carriére, and M. J. Gerry, "A GTD-based parametric model for radar scattering," *IEEE Trans. Ant. & Propag.*, vol. 43 (10), pp. 1058–1067, Oct. 1995.

[8] K-T. Kim, D-K. Seo, and H-T. Kim, "Efficient radar target recognition using the MUSIC algorithm and invariant features," *IEEE Trans. Ant. & Propag*, vol. 50 (3), pp. 325–337, Mar. 2002.

RATIONAL SYNCHRONIZATION OF MICROWAVE OSCILLATORS FOR PHASE-NOISE IMPROVEMENT

S. Ver Hoeye, P. Moreno, D. García, M. Fernández, L. F. Herrán, and F. Las Heras

Department of Electrical Engineering, University of Oviedo
Gijón E-33204, Spain
Tel.: +34 985 182616; Fax.: +34 985 182466; E-mail: sverhoeye@tsc.uniovi.es

Abstract

A new technique for phase-noise reduction in microwave oscillators is presented, based on the synchronization with an external generator at a rational ratio. A design of a synchronized oscillator at the ratio 2/5 is presented, with the simulations and measurements of the synchronization bands. A good improvement of the free-running oscillator phase noise has been achieved.

1. Introduction

Signal generators are one of the most needed elements in modern communication systems. For the implementation of signal generators which generate a time-periodical signal, free-running oscillator circuits are generally an interesting choice. Oscillators used in communication systems generally have very strict phase-noise specifications, which not always can be satisfied by simple configurations of these circuits. In order to reduce the phase-noise generally the oscillator circuit is incorporated in a phase-locked loop or is synchronized by an external generator with very low phase-noise content. In communication systems where a large number of time-periodical carrier signals are required at different frequencies, it is expensive to obtain low phase-noise production in all the carrier signals.

If synchronization by an external generator is used for the phase-noise improvement in a multi-carrier system, it is possible to reduce the number of low phase-noise external reference generators when there exist for multiple carrier signals a different rational ratio between their free-running frequencies and the reference frequency. Then, with a lower number of the required external low phase-noise generators the total cost of the multi-carrier system is reduced.

In this work, a new technique is presented for the phase-noise reduction in microwave oscillators, based on the synchronization with an external generator at a rational ratio, and is illustrated through the design of a 2.9 GHz oscillator synchronized at the ratio 2/5, with the purpose to reduce the number of external low phase-noise generators in a transmitter-receiver system.

2. Rational Synchronization of Oscillators

When an external generator at frequency ω_s is connected to a free-running oscillator at frequency ω_0, a synchronized behaviour is obtained for rational values of the rotation number *r*:

$$r = \frac{\omega_s}{\omega_0}$$

For an arbitrary (non rational) value of *r*, the circuit is working in a quasi-periodic regime at the two fundamental frequencies ω_s and ω_0, with ω_0 the self-oscillation frequency, slightly modified under the influence of the synchroniza-

tion generator. The resulting steady-state solution represented in the state space fills a torus surface [1]. Tuning the frequency of the input generator, for rational ratios *r* = m/n (m, n integer values), the m^{th} harmonic component of ω_0 synchronizes with the n^{th} harmonic component of ω_s. The synchronized solution forms a single closed trajectory in the state space, attracting all the former trajectories of the torus. The synchronization range is delimited by two saddle-node bifurcations [1], and increases with increasing synchronization power P_s. The synchronization range reduces strongly for higher values of m and n [2], and the synchronization phenomenon is difficult to observe experimentally.

3. Circuit Design

Due to the expected narrowness of the m/n synchronization bands, the free-running oscillator must be controllable in frequency. The circuit topology of the rationally synchronized voltage controlled oscillator (VCO) is presented in Fig. 1. The transistor is an ATF36077. The oscillation start-up conditions are satisfied at the drain port through series feedback (including a varactor diode) at the source port. The synchronization generator is connected to the circuit through an input-filter at ω_s. Also an output filter at ω_0 is used in order to reject the synchronization frequency. The circuit parameters have been optimized in order to obtain a 2.9 GHz self-oscillating frequency, employing an auxiliary generator (AG) at the frequency $\omega_{AG} = \omega_0$, and with voltage V_{AG} and phase Φ_{AG} [3].

4. Nonlinear analysis of the rationally synchronized oscillator

For the analysis of the synchronized circuit at the ratio *r* = 2/5, the synchronization generator is connected to the circuit with frequency ω_s and constant power P_s and phase Φ_s. The synchronization ranges of the 2.9 GHz VCO are analyzed by tracing the synchronization loci for different values of the synchronization power P_s. For this, a harmonic balance simulation is used with a Fourier-series expansion at the fundamental frequency $\omega_f = \omega_0/5$. With this selection of ω_f, the self-oscillation frequency is $\omega_0 = \omega_{AG} = 5\omega_f$ and the synchronization frequency is $\omega_s = 2\omega_f$. The synchronization loci are obtained, carrying out a sweep in $\Delta\Phi = \Phi_{AG} - 5/2\ \Phi_s = \Phi_{AG}$ ($\Phi_s = 0$) between 0 and π, calculating for each point of the sweep, the two variables V_{AG} and the self-oscillation frequency $\omega_0 = \omega_{AG}$, in order to satisfy the condition $Y_{AG} = 0$, with Y_{AG} the admittance represented by the AG [3]. Note, that for this sweep in $\Delta\Phi$, a 2π phase variation of the harmonic component at $2\omega_0 = 5\omega_s$ is obtained. The resulting synchronization loci for different values of P_s are shown in Fig. 2.

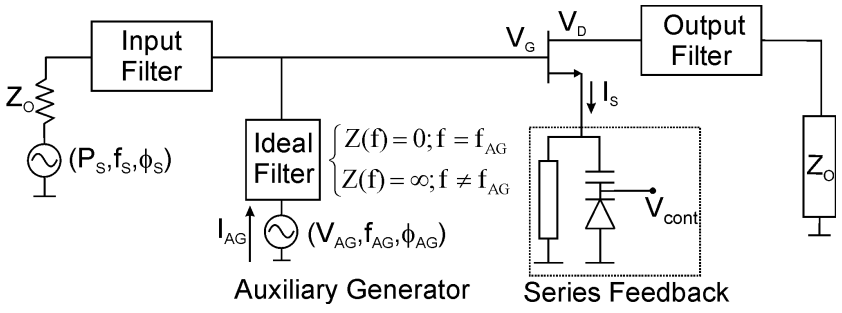

Figure 1. Circuit topology of the rationally synchronized voltage controlled oscillator

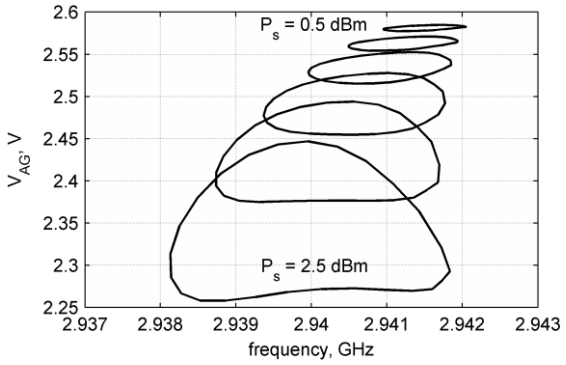

Figure 2. Synchronization loci for different values of the synchronization power P_s

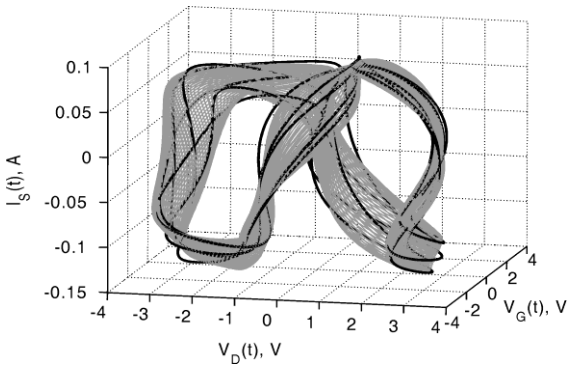

Figure 3. Representation of the synchronized (black line) and unsynchronized (grey line) solutions in a state-space

For higher values of the synchronization power P_s, wider synchronization ranges have been found. In Fig. 2, also a small shift of the self-oscillating frequency can be observed for different values of P_s, which indicates that the varactor voltage should be modified in order to obtain a synchronization loci centred at 2.9 GHz. The synchronized and unsynchronized solutions in time domain are represented in a state-space in Fig. 3. The variables employed in the representation are the drain voltage V_D, the gate voltage V_G and the source current I_S. In the state-space, the quasi-periodic state that corresponds with the unsynchronized solution fills a torus surface (grey lines). When the system approaches the synchronized state, certain region on the torus becomes more attractive than the rest of the surface, and the orbit spends more time around it. In the synchronized state (black orbit in Fig. 3), both frequencies are harmonically related, and there is a closed orbit that attracts all the trajectories on the former torus. This orbit closes over itself after one period of the fundamental frequency $T_f = 1/f_f = 5/f_0 = 2/f_s$, which corresponds with five periods of the self-oscillating component and two periods of the component at the synchronization frequency.

5. Experimental results

The synchronized circuit has been manufactured and measured. Fig. 4 shows the comparison between the simulated and the measured synchronization range versus the synchronization power. Fig. 5 shows the comparison between the output spectrum of the free-running and the synchronized oscillator, in a reduced span of 1 MHz. An important reduction of the phase noise is observed when the oscillator is synchronized. The circuit did not unlock in long term measurements of two days and was stable in the temperature range of 0-45ºC.

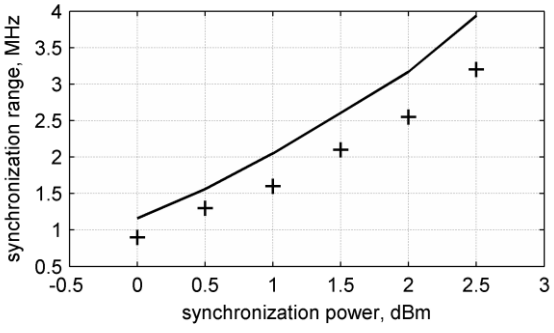

Figure 4. Synchronization range versus the synchronization power ——— simulated + + + + measured

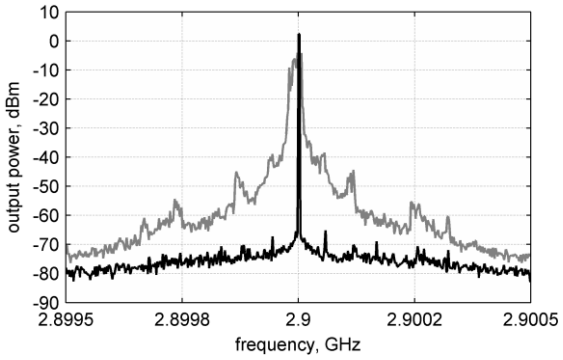

Figure 5. Output spectrum of the free-running and the synchronized oscillator. Grey line: free-running oscillator. Black line: synchronized oscillator

6. Conclusion

A new technique for the phase-noise reduction of a microwave oscillator, based on the rational synchronization with an external generator, has been illustrated through the synchronization of a 2.9 GHz voltage controlled oscillator at the ratio 2/5. The synchronization range has been obtained through a harmonic balance simulation of the circuit and experimentally verified by measurements. An important phase-noise improvement has been observed in synchronized operation.

Acknowledgments

This work was supported by the "Ministerio de Educación y Ciencia" of Spain, under Grant TEC2005-03563, and by the "Gobierno del Principado de Asturias" under Grant No. PC04-49.

References

[1] J. Guckenheimer, and P. Holmes, "Nonlinear oscillations, dynamical systems and bifurcations of vector fields", *Springer-Verlag*, New York, 1990.

[2] X. Zhang, X. Zhou, B. Aliener, and A. Daryoush, "A study of subharmonic injection locking for local oscillators", *IEEE Microwave and Guided Wave Letters*, March 1992, Vol. 2, No. 3, March 1992, pp. 97-99.

[3] S. Ver Hoeye, A. Suárez, and J. Portilla, "Techniques for oscillator nonlinear optimization and phase-noise analysis using commercial harmonic-balance software", *In proceedings of IEEE Int. Microwave Symposium*, June 2000, Boston, pp. 95-98.

BROADBAND SATELLITE SCP-RPSC COMMUNICATIONS – THE NEW CHANCE FOR THE TELEMEDICINE

Assos. Prof. Veselin Demirev

Radiocommunication Department, TU-Sofia, Kl. Ohridski blv. № 8 , 1756-Sofia,
Tel. 3592-965-26-60, e-mail:demirev_v@tu-sofia.bg

Abstract

A new technology, named SCP-RPSC, was developed recently for broadband interactive satellite fixed and mobile terminals. It uses entirely new approach, based on random phase antenna arrays and correlation processing in the receiver. The goal of this report is to discuss the possibilities and the advantages of the implementation of SCP-RPSC technology in satellite communications, particularly as telemedicine subscriber terminal front end equipment.

Keywords: *Spatial Correlation Processing Random Phase Spread Coding Telemedicine*

1. Introduction

The most important use of satellite technology in the health and medical sectors in the near term will be in broadcasting information to the broad public on such matters as how to combat the spread of infections, nutrition, ways to cope with epidemics, finding access to medications or vaccinations, and so on [1]. Today these applications have already saved millions of lives in Asia, Africa, South and Central America, and other parts of the world. The second wave of satellite-based telehealth applications will come as a result of satellite and Internet-based training for medical practitioners and researchers in remote locations. These medical personnel can use these systems to learn the latest treatments, order needed vaccines, train their nurses and medical aides, and otherwise support their operations even in the most isolated locations. Satellite networks now allow remote clinics—whether in a jungle or an off-shore oil rig—to train their nurses, request diagnoses based on high quality video scans, and otherwise assist their operations. Eventually satellite networks will be able to provide a variety of medical services to patients in remote locations as a matter of routine.

One of the biggest technical problems of Satellite Communication Ground Systems (SCGS) for telemedicine is the antenna system. The need to change the polarisation, to select one of several Geo Stationary Orbit Satellites (GEO,s) positions, as well as the requirements for mobile reception, low price and mass market production leads to unsolved by traditional antennas problems. The required antenna gain is above 36 dBi, corresponding to half power beam width of about 4 degrees. Even in fixed telemedicine applications the pointing of the antenna beam to the selected satellite is not easy. Often the base of the antenna support equipment is not stable and due to different factors as strong winds, human activities ets. the satellite reception is a problem. Phased arrays have been used for many years to achieve electronic beam control in applications ranging from communications to radar. An adaptive array is a variation on this which involves the use of the output signals of the array elements in a feedback arrangement to control the phase shifters.

This has found application in communications systems where more sophisticated beam control is required to achieve direction finding and the formation of multiple nulls to avoid jamming signals. Both such arrays depend on a central control system and suffer of many disadvantages when high gain antenna arrays with thousand radiators are employed.

The solving of the SCGS antennas problems needs entirely new approach, which is subject of several years research activity of the author [2], [3], [4]. The name of the new technical solution is Spatial Correlation Processing – Random Phase Spread Coding (SCP-RPSC).

2. SCP approach – objectives and principles of operation

The main objectives of the SCP technology [2], [3] are:

- To receive one or more radio signals coming from one or several spatially distributed sources (satellites), insuring high gain of the antenna systems and using fixed or mobile receiving terminals, equipped with SCP signal processing system.
- To ensure spatial selectivity high enough to cancel the same frequentcy channel interference, coming from different space directions, using simple one-channel receiver and patented signal processing principle.

The objectives stated above are achieved by a patented method for radio communications, which proposes application of additional pilot signal transmitted in the band of information signals and available in the receiver by one of the known methods for access (for example CDMA-Fig.1). SCP receiver terminal is equipped with antenna array with equal in amplitude and random in phase aperture excitation. The phase shifts among the signals, coming from the antenna elements, are random at the antenna output, regardless of the information source direction. These random phase spread signals correlate with the recovered pilot signal, phase spread in the same manner, in the Signal recovery unit. Since the pilot comes from the same direction and propagates in the same random environment to the antenna output, it has the same phase spread signature as the information one. The result of the correlation process between the pilot and information signals is the recovered information signal at base band. The signals coming from other satellites will propagate in different random environment. Their phase spread will be different from those of the chosen pilot and will not correlate with it during the signal processing. This lack of correlation in fact ensures the spatial and polarization selectivity of the SCP system.

One of the main parts of the SCP system is the random phase antenna. In principle all kind of antenna arrays could be used, but for Ku band particular suitable for this purpose is the Radial Line Slot Antenna (RLSA). Until now it is used as phased array for fixed satellite reception.

The main features of the SCP approach in the particular telemedicine applications are:

- Simple, cheap and flat passive radial line antenna, suitable for mass production in Ku and Ka frequency bands and for mounting on cars and unstable bases.
- One channel convenient microwave receiver with simple signal processing.
- Omnidirectional for the cooperative satellite, but with high figure of merit G/T.
- Selection of different satellites and polarizations by PN-codes.
- Applications in existing S-DVB systems with minor modifications of the ground transmitters, compatible with the existing satellite transponders.

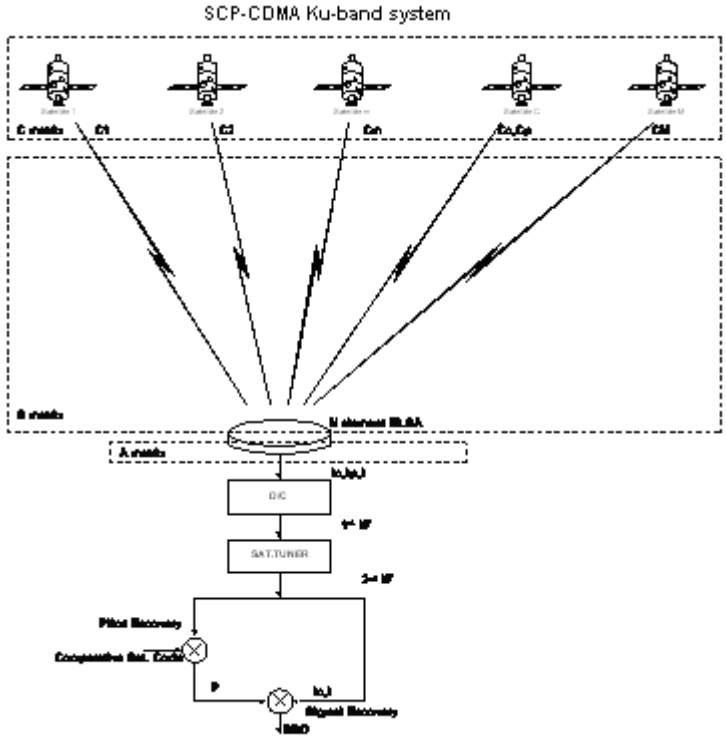

Fig. 1. Block scheme of a SCP-CDMA system

The practical implementation of the SCP approach leads to the problem of pilots transmission through the same propagation environment as that of the cooperative information signals. The CDMA approach matches in the best way to the pilots transmission requirements. The frequency spectrum of a SCP-CDMA system is shown in the Fig. 2 below:

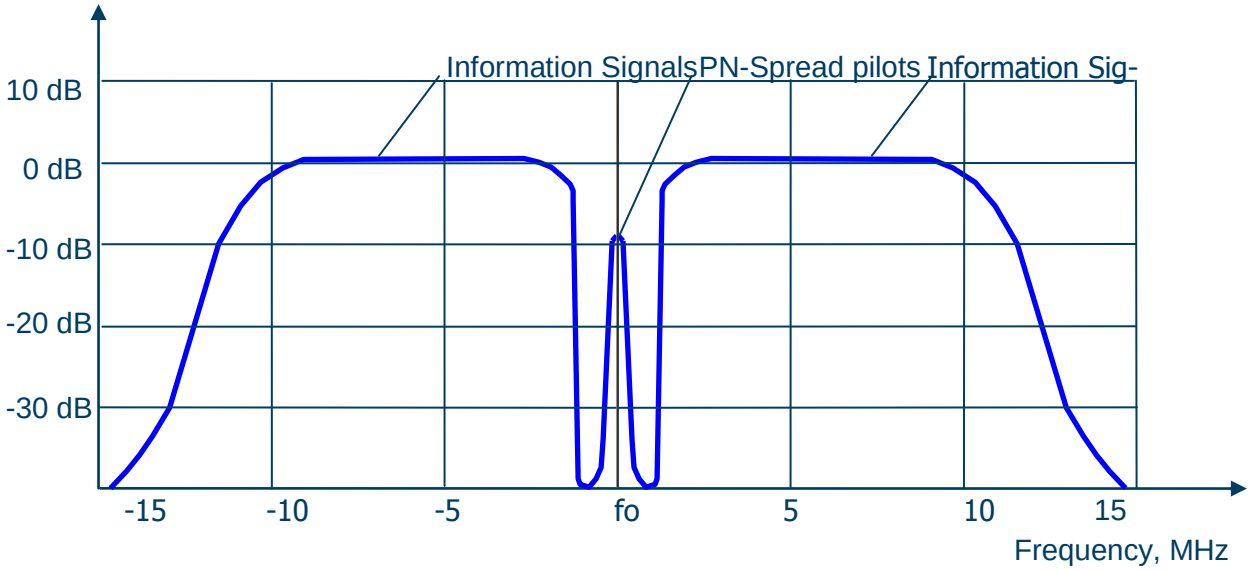

Fig. 2. Frequency spectrum of a SCP-CDMA system

3. SCP-RPSC approach

3.1. Introduction

The idea to use the SCP principle in transmit mode (Ref. 4) was born during the SCP project research. The transmitting antennas, as well as the receiving random phase antenna arrays in SCP technology are pure passive, without any active or nonreciprocal elements. The specific SCP processing is situated in the receiver. According to the basic electromagnetic antenna lows the replacement of the passive transmitting antenna with passive random phase antenna array in the transmitter, and vice versa in the receiver should not change the system working principles and system parameters. The transmitted by the random phase antenna array signals have specific phase spread. It can be considered as random spatial coding. That is why the term SCP-RPSC (Random Phase Spread Coding) will be used instead SCP, transmit in the text below. The signals and the propagation matrix components in the SCP-RPSC case will be denoted with "t".

3.2. The main SCP-RPSC features

The main features of the SCP technology in receive mode are listed in the text above. The proposed SCP-RPSC system will have the following additional features:

- Providing full duplex interactive system with one simple and cheap transmit-receive antenna.
- The transmitted random poly-phase spread signals will not cause significant harmful interference to the conventional satellites, using the same frequency channels. The interference will be similar to that, caused by the sidelobes of a phased antenna array with random inter elements spacing.
- The transmitted random poly-phase spread signals are uniformly radiated in the space above the antenna. Several satellites, equipped with the same SCP receivers and providing space diversity, receive them. The knowledge of the receiving satellites positions for the transmitting equipment is not necessary (as it is for a conventional satellite earth station).
- The SCP-RPSC approach could be a breakthrough technology, leading to unpredictable increase of the frequency reuse factor in satellite and terrestrial wideband networks. Close situated subscriber terminals could communicate with terrestrial or satellite base stations, using the same frequency channel without interference. The isolation between the terminals will be provided by their specific random phase spread coding, due to their specific random design.

3.3. Background of the SCP-RPSC technology

A block scheme of a SCP-RPSC satellite system is shown in fig. 3, where:

(1) is a transmitter of SCP signals (modulated information signals and CDMA-spread pilot signals).

(2) is a Random Phase Antenna Array (RPAA).

(3) is a conventional microwave receiving antenna.

(4) is a conventional one channel receiver with IF output.

(5) is a SCP Pilot recovery unit.

(6) is a SCP Signal recovery unit (correlator).

(7) is a baseband signal processing equipment.

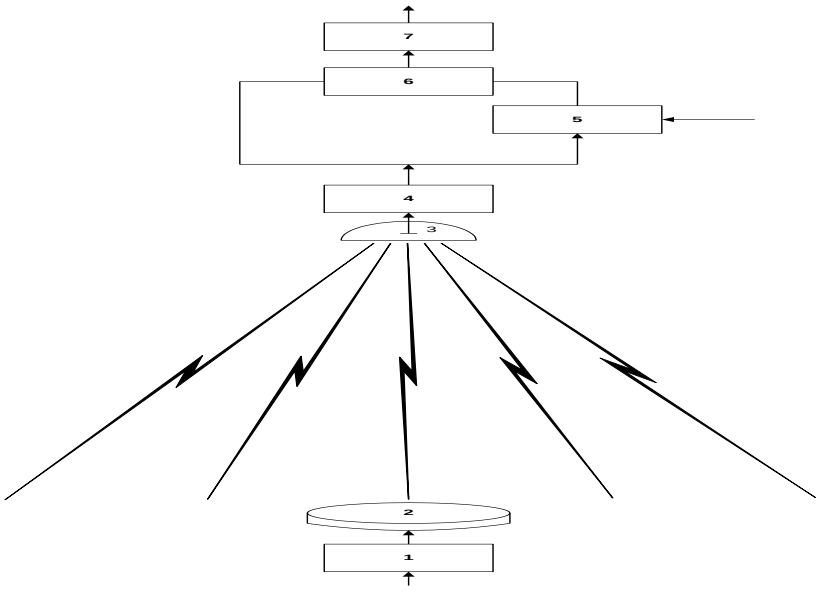

Fig. 3. Block scheme of a SCP-RPSC system

4. Conclusions

The practical SCP-RPSC principles implementations in transmit and receive mode will drastically change the existing paradigm in the satellite communication business in general. Many of the existing problems of the proposed LEO, MEO and GSO satellite systems, dealing with frequency and orbital resource sharing, beam pointing, beam shadowing, etc., will be solved successfully. The SCP-RPSC technology will be particularly useful for the future telemedicine applications in all kinds of their aspects.

5. References

[1]. J. Pelton, R. Oslund, P. Marshall, *Communication Satellites – Global Change Agents*, Laurence Elbaum Associates, London, 2004.

[2] V. Demirev, "SCP technology – the new challenge in broadband satellite communications", *ICEST,04 Proceedings of Papers*, Bitola, Macedonia, vol.1, pp. 159-162, June 16-19, 2004

[3] V. Demirev, A. Efremov, "SCP-CDMA GSO,s system proposal", *ICEST,04 Proceedings of Papers*, Bitola, Macedonia, vol.1, pp. 163-166, June, 16-19, 2004

[4] V. Demirev, "Review of SCP-RPSC technology", *ICEST,05 Proceedings of Papers*, Nis, Serbia and Montenegro, vol. 2, pp.630-633, June 29-July 1, 2005.

AN INVESTIGATION ON PROPAGATION AND ABSORPTION OF ELECTROMAGNETIC SIGNALS THROUGH BIOLOGICAL MEDIA

Dimiter Tz. Dimitrov

Technical University of Sofia
8, Kliment Ohridsky str., 1000 Sofia, Bulgaria
Tel.+359 2 9652278, E-mail:dcd@tu-sofia.bg

Abstract

A basic knowledge of biological material properties, their uniqueness, and their variability among living systems may provide a basis for the exploitation of electromagnetic interaction mechanisms. The macroscopic approach deals with the whole biological material exposed to electromagnetic fields generated by the exogenous fields. This approach requires complete knowledge of the electromagnetic properties of the material. Ability to solve Maxwell's equations with the appropriate boundary conditions is also required.

A mathematical analysis of the processes of propagation and absorption of electromagnetic signals in the live tissues have been done in the paper taking in account some specific values of the conductivity of biological materials σ, the real part of the complex relative permittivity of biological materials ε' and the imaginary part of the complex relative permittivity of biological materials ε''.

The principal results of present investigation is connected with mathematical description of the processes of propagation and absorption of electromagnetic signals in the live tissues.

1. Introduction

It's known [1], [2], [3] that when electromagnetic radiation contacts matter, it interacts with atoms in the medium and behaves like particle in a way and like a wave in another way. Particle-like behaviors include reflection, scattering and absorption [4]. The wavelike behaviors include reflection, refraction, transmission, diffraction and absorption of electromagnetic signals [5], [6], [7]. The effect of the radiation on matter depends on many factors including wavelength components of radiation, the sending medium, the polarization components of the radiation and the angle of incidence [8], [9]. A mathematical analysis of propagation of electromagnetic signals through biological media is described in the paper.

2. Propagation of electromagnetic signals through biological media

The propagation of electromagnetic waves in a biological medium Figure (1) can be studied mathematically by solving Maxwell's equations under appropriate boundary conditions.

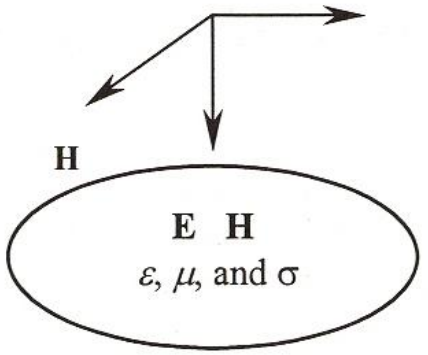

Figure 1. A biological body under EM radiation

These equations are very powerful, but complicated and difficult to solve. For simplicity, it's possible to assume that a biological medium is infinite in extent, source-free, isotropic, and homogeneous. The medium is isotropic if ε is a scalar constant, so **D** and **E** are the same in every direction. A homogeneous medium is one for which ε, μ and σ are constant. For this case, Maxwell's equations become:

$$\nabla x\vec{E} = -\frac{\partial \vec{B}}{\partial t} \qquad (1)$$

$$\nabla x\vec{H} = \vec{J} + \frac{\partial \vec{D}}{\partial t} \qquad (2)$$

$$\nabla .\vec{B} = 0 \qquad (3)$$

$$\nabla \vec{D} = 0 \qquad (4)$$

Further, since the medium is assumed to be isotropic, its permittivity, permeability, and conductivity are scalars. In case the medium is homogeneous, these parameters are constants.

In order to solve this set of simultaneous equations for the vectors **E** and **H**, the vector **H** may be eliminated from the equation in the following way:

$$\nabla x(\nabla x\vec{E}) = -\mu \frac{\partial}{\partial t}(\nabla x\vec{H}) =$$

$$= -\mu \frac{\partial}{\partial t}(\sigma\vec{E} + \varepsilon \frac{\partial \vec{E}}{\partial t}) =$$

$$= -\mu\sigma \frac{\partial \vec{E}}{\partial t} - \varepsilon\mu \frac{\partial^2 \vec{E}}{\partial t^2} \qquad (5)$$

Using the vector identity, the equation determining the vector **E** comes out to be

$$\nabla x\nabla x\vec{E} = \nabla(\nabla .\vec{E}) - \nabla^2 \vec{E} \qquad (6)$$

and using Equation (4):

$$(\nabla^2 - \mu\sigma \frac{\partial}{\partial t} - \mu\varepsilon \frac{\partial^2}{\partial t^2})\vec{E} = 0 \qquad (7)$$

Similarly, by eliminating E from the Maxwell's equations, it may shown that H satisfies the equation:

$$(\nabla^2 - \mu\sigma \frac{\partial}{\partial t} - \mu\varepsilon \frac{\partial^2}{\partial t^2})\vec{H} = 0 \qquad (8)$$

In view of the fact that equations governing **E** and **H** in the biological material (Maxwell's equations) are linear and keeping in mind that any arbitrarily time-varying function can be expressed as a sum of number of sinusoidal functions, time dependence of the fields, **E** and **H**, can be given by the factor $e^{j\omega t}$ so that

$$\frac{\partial}{\partial t} \equiv j\omega \text{ and } \frac{\partial^2}{\partial t^2} \equiv -\omega^2$$

Using both relationships in Equation (7), the wave equation becomes:

$$\nabla^2 \vec{E} + \gamma^2 \vec{E} = 0 \qquad (9)$$

where:

$$\gamma^2 = \omega^2 \mu\varepsilon - j\omega\mu\sigma =$$

$$= \omega^2 \mu\varepsilon_0 (\varepsilon' - j\frac{\sigma}{\omega\varepsilon}) = \frac{\omega^2}{c^2}(\varepsilon' - j\varepsilon'') \qquad (10)$$

where:

σ is conductivity of biological materials;

ε' is the real part of the complex relative permittivity of biological materials;

ε'' is the imaginary part of the complex relative permittivity of biological materials;

ε_0 is the absolute permittivity

$$\varepsilon'' = \frac{\sigma}{\omega\varepsilon_0}$$

c is the free space velocity ($3x10^8 \, m/s$) and γ is the propagation constant. This

is, in general, a complex quantity and may be written in the form

$$\gamma = \alpha + j\beta \qquad (11)$$

where the attenuation constant is:

$$\alpha = \frac{\sqrt{2c}}{\omega\sqrt{\varepsilon'}\left(\sqrt{1+\left(\frac{\varepsilon''}{\varepsilon'}\right)^2}+1\right)^{1/2}} \qquad (12)$$

for $\frac{\varepsilon''}{\varepsilon'} \le 1$:

$$\alpha = \frac{\omega\sqrt{\mu\varepsilon}}{\sqrt{2}}\left(\frac{\varepsilon''}{\varepsilon'}\right) \qquad (13)$$

and the phase constant in radians per meter is

$$\beta = \frac{\sqrt{2}c}{\omega\sqrt{\varepsilon'}\left(\sqrt{1+\left(\frac{\varepsilon''}{\varepsilon'}\right)^2}-1\right)^{1/2}} \qquad (14)$$

for $\frac{\varepsilon''}{\varepsilon'} \le 1$

$$\beta = \omega\sqrt{\mu\varepsilon}\left(1+0{,}125\left(\frac{\varepsilon''}{\varepsilon'}\right)^2\right) \qquad (15)$$

Using Equation (15), the wavelength λ can be determined by

$$\lambda = \frac{2\pi}{\beta} \qquad (16)$$

If the incident wave is a linearly polarized uniform plane wave traveling along the z-direction, then Equations (7) and (8) are of the form:

$$\vec{E} = E_i e^{-\alpha z} e^{j(\omega t-\beta z)}\vec{i}_x \qquad (17)$$

$$\vec{H} = H_i e^{-\alpha z} e^{j(\omega t-\beta z)}\vec{i}_y \qquad (18)$$

where $\left|\vec{E}_i\right| = \eta\left|\vec{H}_i\right|$

The intrinsic impedance of biological material η is given by

$$\eta = \sqrt{\frac{\mu}{\varepsilon}}\left(1-0{,}378\left(\frac{\varepsilon''}{\varepsilon'}\right)^2 + j0{,}5\left(\frac{\varepsilon''}{\varepsilon'}\right)\right) \qquad (19)$$

The Poynting vector, that is, the power flowing per unit area of cross section (W/m^2), gives the power density associated with an EM wave can be calculated:

$$P_i = \frac{\left|\vec{E}_i\right|^2}{2\eta} \qquad (20)$$

3. Absorption of electromagnetic signals in the biological materials

It's well known that at radio frequencies, biological tissues behave like solutions of electrolytes that contain polar molecules. RFR interacts with biological systems by way of ionic conduction (oscillation of free charges) and rotation of polar molecules of water and protein relaxation. Absorbed RF energy is transformed into kinetic energy of molecules, which is associated with a rise in temperature of the irradiated tissues.

In order to understand the factors influencing the rise in body temperature due to RF absorption, it is useful to study the different heat pathways within the body. The heat may be transferred to the environment only after it is first transferred to the body surface. This heat transfer may be accomplished by three mechanisms: thermal conduction, thermal radiation, convection, and sweat evaporation.

Thermal conduction is the process in which heat transfer takes place by molecular diffusion. The amount of heat energy flowing per second per unit area is proportional to the temperature gradient. Body tissues are quite poor thermal conductors with values of conductivity between 2-10 cal/min/m/°C.

Thermal radiation is the heat loss due to radiation from the surface of the human body.

Convection is the process in which heat is transferred by the simultaneous action of molecular diffusion and mixing motion.

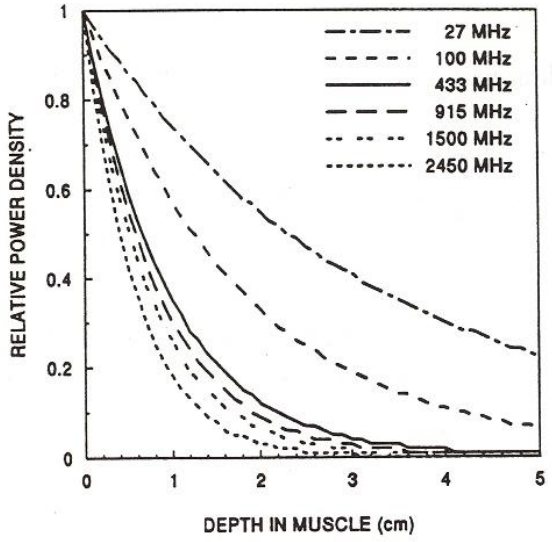

Figure 2. Power absorption in muscle as a function of depth at different frequencies

Evaporation is the heat loss due to evaporation at the surface per unit area (including sweat and insensible perspiration), and it depends on the arterial blood flow, the wind speed, and the humidity.

Sweating is controlled by the central neural integrative mechanism, which receives signals from the thermosensitive sites within the body.

Temperature differences, which would exist in the absence of blood flow, are equalized by the blood flow. The blood flow also controls the effective body insulation through constriction expansion of the cutaneous capillaries, so that the distance the heat has to flow through the superficial layer to the superficial epidermis increases or decreases accordingly.

A nonuniform distribution of absorbed power is a well-established fact [ ], which may lead to involved interactions. In some exposure situations, only certain parts of the body are absorbing RF power causing nonuniform heating, which is generally referred to as hot spots.

It is observed from Equation (17) and (18) that the wave gets attenuated as it propagates in the biological material along the z-axis. As shown from Figure 2, at a given depth uses of lower frequency results in a higher power density. It is also clear that a given power density is achieved at a greater depths in the muscle than that for a higher frequency. Not shown in Figure 2 is that penetration depth at about 30 GHz and higher is largely confined to the outer layers of the skin (much like for sunlight).

The energy is transferred from the applied E field to the material in the form of kinetic energy of charged particles. The rate of change of the energy transferred to the material is called the absorbed power. This power is also called power transferred, but from the bioelectromagnetics point of view, the term specific absorption rate (SAR) is the preferred one. SAR is a quantity properly averaged in time and space and expressed in watts per kilogram (W/kg). SAR values are of key importance when validating possible health hazards and setting safety standards

For steady-state sinusoidal fields, the time-averaged absorbed power per unit volume P_α is given by

$$P_\alpha = \sigma \left|\vec{E}\right|^2 \qquad (21)$$

where $\left|\vec{E}\right|$ is the root-mean-square (RMS) magnitude of the **E**-field at certain point in the material. To find the total absorbed power in a material, the power calculated from Equation (21) must he calculated at each point inside the body and integrated over the volume of the body. Figure 2 shows power absorption in muscle by a plane wave as a function of depth at different frequencies.

4. Conclusion

1. A mathematical analysis of propagation and absorption of electromagnetic signals through the biological media is described in the paper.

2. Some important equations (12), (15) and (19) have been obtained in the paper.

3. The obtained theoretical conclusions can be used as the base conclusion for the next investigation on SAR.

References

[1] Lin, J. C., (ed.), Electromagnetics in Biology and Medicine, Review of Radio Science, 1993-1996, Oxford University Press, London, UK, 1996.

[2] Stuchly, M. A., Biological Effects of Radiofrequency Fields, Proceedings of the International Non-Ionizing Radiation Workshop, Melbourne, Australia, 5-9 April,1988.

[3] Durney, H. D., and D. A. Christensen, Basic Introduction to Bioelectroinagnetics, CRC Press, Boca Raton, FL, 1999.

[4] Jordan, E. C., and K. G. Balmain, Electromagnetic Waves and Radiating Systems, Prentice Hall, Englewood Cliffs, NJ, 1968.

[5] Robert, P., Electrical and Magnetic Properties of Materials, Artech House, Norwood, MA, 1988.

[6] Schwan, H. P., Interaction of Microwave and Radio Frequency Radiation with Biological Systems, IEEE Transactions on Microwave Theory and Techniques 19, pp. 146-152, 1971.

[7] Roberts, J. E. and H. F. Cook, Microwave in Medical and Biological Research, British Journal of Applied Physics 3, pp. 33-40, 1952.

[8] Pressman, A. S., Electromagnetic Fields and Life, Plenum Press, New York, NY, 1970.

MODELING THE MOVING OF CHARGES IN HOMOGENOUS MAGNETIC FIELD

Prof. Dr. Dimiter Dimitrov
dcd@tu-sofia.bg, +359 2 9652278

Hristo Hristov
hristov@tu-sofia.bg, +359 898 718196
Technical University of Sofia, Bulgaria

Abstract

For years, the magnetic field finds great application for medical purposes. Its beneficial influence on humans is an established, though not particularly analyzed, fact. Nowadays, when the computer modeling of processes is coming in strong, it is opening up new vistas for us to provide a set of answers, concerning the magnotherapy, as well as to bring the magnetic fields into optimum use for people. The present article puts forward the concept and the laws that provoke the positional fluctuation and the speed of the charged particles, under the impact of homogeneous electromagnetic field.

Introduction to the problem

The main source of pain in number of diseases or contusions is the formation of ionic accumulations. They represent amassments of ions with equivalent charge, concentrated in a small area. In the human tissue there are lots of liquids that dissociate their molecules into ions with opposite charge (counter-ions) due to the chemical phenomenon – *electrolyte dissociation*. In normal condition, these ions are divided in relatively equal shares in the human tissue and there exists no tension between the particles [1], [2]. However, some contusions and diseases operate so that the ions could constitute ionic depots, in between which exists tension. The tension in question incites a force of strain (in the tissue), therefore: an origination of inner strain, respectively – an initiation of pain [3]. The result of applying the extern magnetic field is dispersing these ionic accumulations, thereby suppressing the pain [4]. How to use technical means to decrease the inner magnetic fields is of interest to us as engineers. An extern magnetic field, which is stronger than the inner one and which could neutralize it (i.e. suppress the ionic depots) is used for that purpose [5]. That particular sort of therapy is called *magnotherapy*. The magnotherapy is a method of the physiotherapy which includes treatment with constant or alternating low frequency magnetic fields. The large range of curative efficacy that provides the magnetic field transmutes the magnotherapy into a future technology. The easy setting of the magnetic applicators, their painless influence, the absence of secondary effects and their affordable price are a prerequisite for this alternative remedial-prophylactic approach to gain wide currency in ambulatory or domestic conditions.

The magnotherapy utilizes a physical phenomenon called the *Lorentz force*. When we put a magnet close to the human body, some magnet forces go through the tissue and they improve the circulation of the blood. This action enables the organism to resuscitate its forces; to overcome the toxicities and the causes of the malaise. As a whole, the application of the magnotherapy could decrease the duration of the treat-

ment and the therapy with approximately 50% less than the foreseen.

Exposition

A weak and constant magnetic field results thanks to tiny magnets. It interacts with the deeper muscle layers and there it stimulates the normal course of the organic processes. The cramps decrease without any medications or other side effects.

The surrounding ambience is enlaced with magnetic fields: some generated by the natural terrestrial magnetism, others – by solar storms or weather changes. There are also magnetic fields created intentionally by electric apparatus (engines, TV-sets, office equipment, computers, micro ovens, etc.). Even the human body gives rise to a magnetic field, generated by chemical reactions of the nerve cells containing ions. The electromagnetic field represents simultaneously an electric and a magnetic field. It is identified as electronic because of the presence of charged particles (i.e. the electrons) and it is acknowledged as magnetic due to circulation of these charged particles. In roughly recent studies, the scientists found that the extern magnetic field could be good for the health – this inference led to the "invention" of the magnotherapy.

The dosage here is crucial, such as the posology of the medicines. Achieving optimum application performance needs good prior research of the practice; of the most advantageous for the human's body values, when exactly the magnetic field gives its most beneficial effect. For the purposes of the charge performance research (under a magnetic field), we've elaborated a program that simulates the process. Its goal is to illustrate the variations of the speed and the position of the charged particle (ion, electron, and proton) under a dynamically alternating and homogenous magnetic field.

The physical model of the system is as follows: two fields act to the charged particle – an electric field (prominent for its electric intensity) and a magnetic field (distinguished by its magnetic induction or magnetic flux density). These two fields vary in time according to a sinusoidal law and they initiate certain forces, which operate on the charges. More specifically, this brings up the Lorentz force, which originates the speed variation and the situation variation of the charge.

The Lorentz force is known from the physics:

$$\vec{F} = q\,(\vec{E} + \vec{v} \times \vec{B}) = q\,\vec{E} + q\,(\vec{v} \times \vec{B}) \qquad (1)$$

q – is used to denote the quantity of the electric charge (C)

E – is used to denote the vector of the electric intensity (V/m),

v – is used to denote the velocity of the charge (m/s)

B – is used to denote the magnetic flux density of the magnetic field (T)

$\times$ stands for cross product of the two vectors. We'll use this formula, whenever both (electric and magnetic) fields are active. And in case when the electric field value comes up to zero (or is insufficiently small, hence the above-mentioned formula takes on a new mode):

$$\vec{F} = q(\vec{v} \times \vec{B}) \qquad (2)$$

We'll use this formula whenever the speed of the charges is generated on a random basis and not due to any given electric field.

After we find out the force, which acts to the charge, referring to Newton's second law, we could calculate the acceleration, which will gain the charged particle. The Newton's second law of motion encloses the following formulation:

$$\vec{F} = m\vec{a} \qquad (3)$$

where *m* represents the mass (kg) and *a* is the vector of the acceleration (m/s^2). From (3) we can express the acceleration:

$$\vec{a} = \frac{\vec{F}}{m} \qquad (4)$$

After calculating the acceleration we can integrate it in time and this way we'll get the change of the velocity for certain time interval (the limits of the integral). It does matter what will be the integration step we'll use – the littler it is, the more points from the trajectory we'll calculate and thus the precision will grow. The formula we'll use is

$$\Delta\vec{v} = \int_{x1}^{x2} \vec{a}dt \qquad (5)$$

The integration in this case is reduced to the integration of the three components of the acceleration vector, which are constant in every one moment of time. Knowing the new value of the velocity of the charge we can calculate how its position has changed. From the equation

$$\vec{S} = \vec{v}t \qquad (6)$$

where *S* represents the track, covered by the charge, *v* represents the velocity and *t* – the time; we can calculate the distance, traveled by the particle. This way we can calculate the alteration of the position of the charge in the time.

To make all these calculations we can use some programming language. The investigation we've made uses the Java programming language (version 1.4). This is a modern object-oriented language, from the third- generation, who has lots of advantages – it is platform independent, has good support form the Internet browsers and is very widespread, portable and secure. One other big advantage of Java is the license under which it's distributed – totally free.

An example of the execution of the program can be seen at the following URL:
http://diplomna-javadoc.hit.bg/applet/applet.html

The aim of the program is to demonstrate how will vary the velocity and the position of one or more charged particles, under the influence of an electromagnetic field. For the research's purposes we've made some presumptions:

- we presume that the electric and the magnetic fields are homogenous in every one point of them and in every one moment of the time.
- we ignore the fact, that every moving in magnetic field particle produces an additional magnetic field around it. This supposition is correct because in the common case the external magnetic field is much more powerful then the one generated by the particle and that's why we can ignore it.

The results of the research we've made could be used to discover the most optimal values and form of the electromagnetic field, so we could use best its potential for better therapeutic effect when treating diseases and contusions. A well-know fact from the medicine is that for every type of treatment it's very important not to let the organism to get used to the therapy. That's why it's absolutely necessary to change the form and the value of the magnetic field which will operate on the object of the treatment. Physiotherapists and medicals can use such type of simulations to choose the most suitable values for the electromagnetic field so that the positive effect will continue as long as possible.

For the development of this simulating program we've created some java classes that describe the electric and the magnetic fields and the appropriate classes for visualization the change of the velocity and the position of the charge. For the magnitude and the

weight of the particle we've used some known form the physics values.

The main screen of the application looks like this:

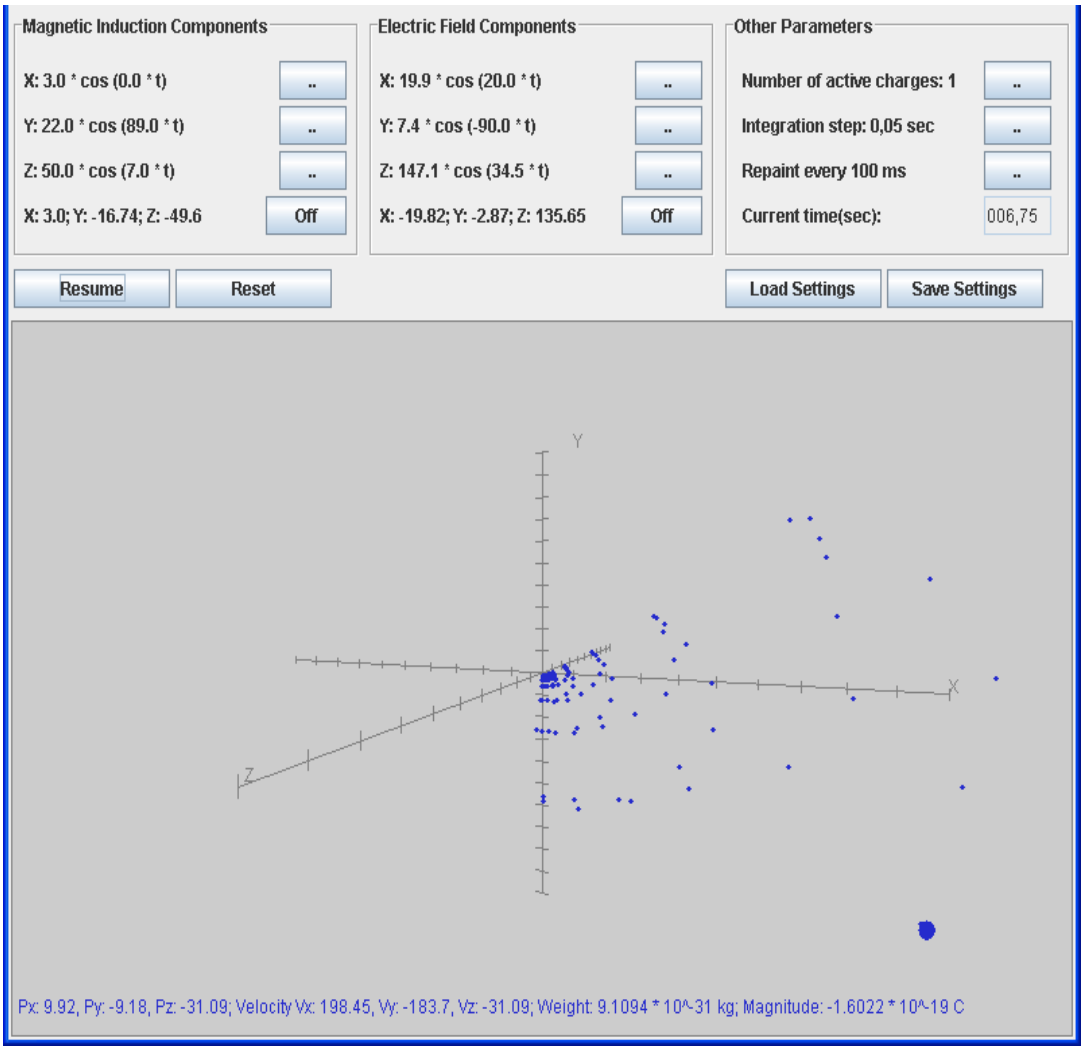

Conclusion

The magnotherapy is a method for curing a great number of diseases and contusions, which makes it very perspective for the future. To use the full potential of this type of therapy it's very important to study it and find the most proper parameters of the health equation. With the temps of progress of the techniques today (and especially those of the computers), we can make successful simulation of the processes that take place in the tissues under the influence of an external magnetic field. These simulations can lead to some conclusions which can optimize the use of magnetic fields. For this purpose we've developed a program for simulating the behavior of the charged particles placed in the influence of external homogenous electromagnetic field. The conclusions that physiotherapists and medicals can reach using such type of simulations can help for more optimal and quick treatment of the patients. In version one of our product we have mentioned the potential of using the computers like our ally in the war with the pain. At this stage of the development of the product, the program has more informational and research nature, then practical use. To be truly helpful for the real cases we will have to

add some functionality like reading the resistance of the tissues, using the real form of the electromagnetic field, include the noises which are around us, etc.

References

[1] http://bg.wikipedia.org
[2] http://www.samozdrav-bg.com
[3] http://www.permahealth.com/bg/informacia.htm
[4] http://library.thinkquest.org/24206/therapies/magnetic-field_therapy.html
[5] Д. Димитров, Комуникационни системи в медицината, Изд. Технически Университет, София, 2005

THE ULTRASONIC TRANSDUCER PREAMPLIFIER NOISE PERFORMANCE

V. Dumbrava, L. Svilainis

Signal processing department, Kaunas University of Technology
Studentu str. 50, LT-51368 Kaunas, Lithuania
T, +370 37 300532; F, +370 37 753998;E,vytautas.dumbrava@ktu.lt / linas.svilainis@ktu.lt.

Abstract

The preamplifier noise performance is important in the case of a medical ultrasonic inspection.

In this paper we analyze the noise by using the complete mathematical model for input stage, incorporating transducer, transformer, operational amplifier and the external passive components. The analysis is used for noise parameters prediction. The theoretical results have been tested experimentally. The system for signal propagation and an absolute noise level measurement over the frequency range has been developed. The experimental results have been used to calculate the noise performance.

The theoretical and experimental investigation confirmed the ability to improve the ultrasonic preamplifier noise performance.

1. Introduction

In medical ultrasonic inspection transmitted power is limited in order to protect the tissue. This will limit transducer reception sensitivity [1-3].

Therefore improving the preamplifier noise response is very important. Noise performance can be defined by absolute noise level, signal-to-noise ratio (SNR), noise figure (NF) [4, 5]. All the above can be analyzed either as the frequency-dependent response or as root-mean-square (RMS) integral over passband.

The input circuitry, the amplifier external components and its topology influence the noise and signal propagation to the output. Transformer introduction between the transducer and the preamplifier input can be used to alter SNR of the input stage [6-8].

In order to analyze the noise performance the mathematical model is needed for complete preamplifier schematics [9, 10].

2. Noise model

The gain bandwidth of modern operational amplifiers is reaching 2GHz, which makes it attractive choice for preamplifier design in ultrasonics. Therefore we limit our investigation to the operational amplifier schematics.

2.1. General preamplifier model

We decided to use the analytical model incorporating both transducer and electronics [7]. Then the noise sources can be separately analyzed.

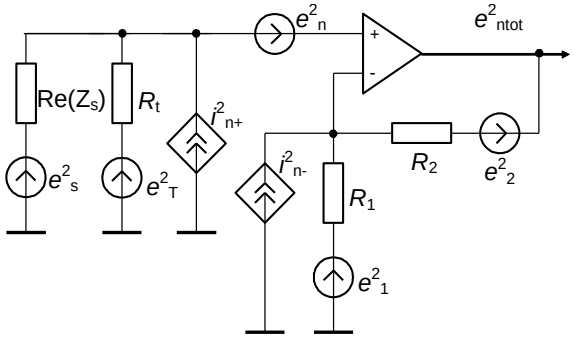

Figure 1. Noise model circuit

The ultrasonic transducer noise and signal transmission is modelled using BVD (*Butterworth-Van Dyke*) model [9]. The noise spectral density of the is input resistance R_t

$$e_T^2 = 4kTR_t\,, \qquad (1)$$

where k is the Bolzmann constant, T is the absolute ambient temperature.

The transducer noise spectral density is determined by the real part of the transducer impedance [4]

$$e_s^2 = 4kT\,\mathrm{Re}(Z_s)\,. \qquad (2)$$

The feedback circuit resistors contribute the noise densities

$$e_1^2 = 4kTR_1\,;\quad e_2^2 = 4kTR_2\,. \qquad (3)$$

Operational amplifier intrinsic noise is modelled using voltage source e_n and current noise sources i_{n+} and i_{n-}. With the amplifier noise gain

$$G = \frac{R_1 + R_2}{R_1} \qquad (4)$$

we get the equation for the output noise density calculation:

$$e_{ntot}^2 = \left|\frac{GR_t}{R_t + Z_s}\right|^2 e_s^2 + \left|\frac{GZ_s}{R_t + Z_s}\right|^2 e_T^2 + \left|\frac{GR_tZ_s}{R_t + Z_s}\right|^2 i_{n+}^2 + G^2 e_n^2 + (G-1)^2 e_1^2 + e_2^2 + R_2^2 i_{n-}^2 \qquad (5)$$

Similar way one can obtain the expression for signal at the amplifier output [5]. Then noise figure [6]:

$$NF = 10\lg\frac{SNR_i}{SNR_o}\,. \qquad (6)$$

where – SNR_i and SNR_o – signal to noise ratio at the at input and output. Optimal source resistance R_{opt} exists minimizing the amplifier NF [4]:

$$R_{opt} = \frac{e_n}{i_{n+}}\,. \qquad (7)$$

For reference, R_{opt} for OPA657 is 3.7 MΩ and 400 Ω for LMH6624.

2.2. Transformer model

In general, transformer application can be justified by three reasons: noise improvement thanks to ability to modify the source impedance, isolation and optimum power transfer thanks to impedance matching. It also allows effective operational amplifier biasing via transformer winding inductance.

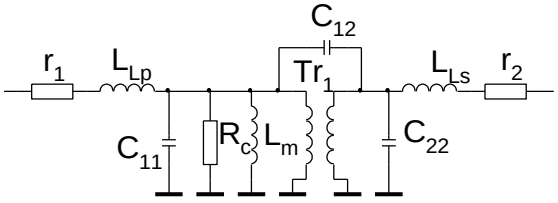

Figure 2. Complete transformer model

Resistance r_1 and r_2 are presenting the losses in the primary and secondary windings, respectively. The core losses are encountered through shunt resistance R_c. The coupling factor defines the level of leakage inductances L_{Lp} and L_{Ls}. The magnetizing inductance L_m represents the effects, associated with final core permeability. Lumped capacitances C_{11}, C_{22} and C_{12} are presenting the distributed capacitances.

3. Modelling results

In order to evaluate the importance and influence of circuit parameters, we now can investigate equation (5) noise components. The preamplifier with and without the transformer are studied.

3.1. Preamplifier noise

We have chosen three amplifiers as representatives of achievable limits. One (LMH6624, BJT amplifier) is presenting the lowest e_n, other (OPA657, FET amplifier) is exhibiting the lowest i_n and the third (AD8009) is a current feedback amplifier. To ignore the R_1 and R_2 noise, e_1 and e_2 has to be 1/3 of e_n contribution. According to the results [3], the optimal values are R_1=10Ω, R_2=1kΩ. The obtained NF for R_t=10 kΩ is presented in Figure 3.

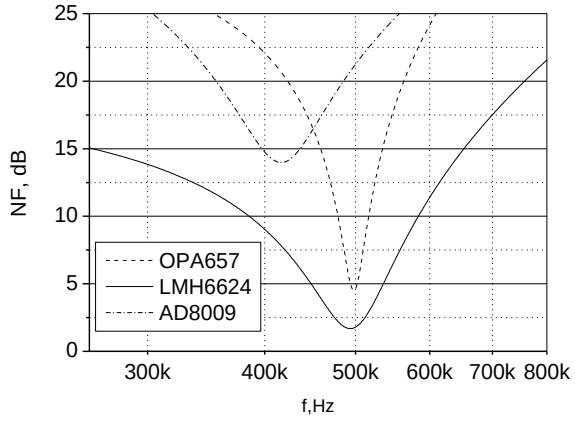

Figure 3. Preamplifier NF vs. frequency

It's clear that in the case analyzed LMH6624 exhibits lowest noise figure.

3.2. Preamp with transformer

We simplify the transformer model and split it depending on transducer output impedance case. In case of low transducer impedance only r_1 and r_2 are used since core losses can be neglected. In case of high transducer impedance, shunt resistance R_c represents the major concern, so it should be taken into account.

3.2.1. Winding losses model

If ultrasonic transducer exhibit low output impedance, only r_1 and r_2 are used and transformer core losses can be neglected. Now the preamp noise model incorporates the transformer *1:n* and it's winding losses.

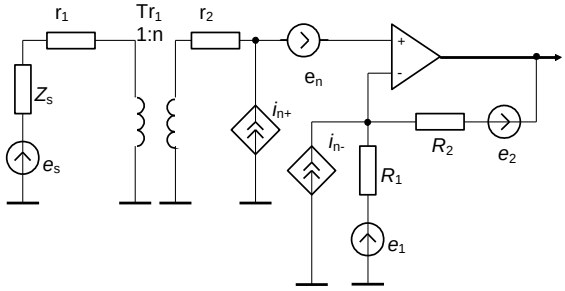

Figure 4. Model for winding losses

The noise spectral density and the signal level at the preamplifier input and output are evaluated as above. Turn to results in our publication [8] for complete explanation.

The noise figure is minimal for optimal transformation coefficient.

$$n_{opt} = \sqrt[4]{\frac{4kTr_2 + e_n^2 + i_{n+}^2 r_2}{i_{n+}^2 \left| Z_s + r_1 \right|^2}} \quad . \qquad (8)$$

It can be seen from the equation above that the optimal turns ratio n_{opt} if winding losses should be taken into account is defined by r_1, and r_2. Usually $4kTr_2 << e^2_n >> i_{n+}r_2^2$ is satisfied, therefore r_2 can be omitted. Figure 5 is indicating the ratio n_{opt} change versus frequency for two transformer winding resistances.

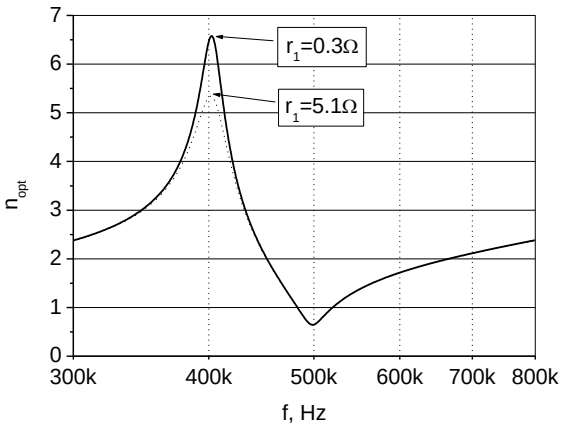

Figure 5. Optimal turns ratio n_{opt}

As can be seen from the Figure 5 n_{opt} is changing in wide range. In practice such transformer is not realizable.

Therefore only one value of *n* can be used. Then the noise figure variation versus frequency and transformation coefficient *n* contour plots get useful for choosing the right turns ratio (refer to Figure 6).

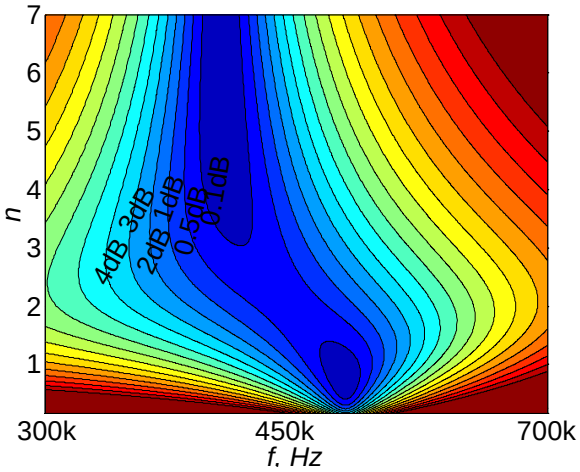

Figure 6. NF vs. frequency and turns ratio for low impedance transducer

Figure 6 indicates that noise figure is degraded due to non-optimal *n.*

3.2.2. Core losses model

If ultrasonic transducer has high output impedance, shunt resistance R_c represents the major concern, so it should be taken into account. Winding losses r_1 and r_2 can be neglected in such case. The resulting noise figure is presented in Fig.7 (for FET) and Fig.8 (for BJT).

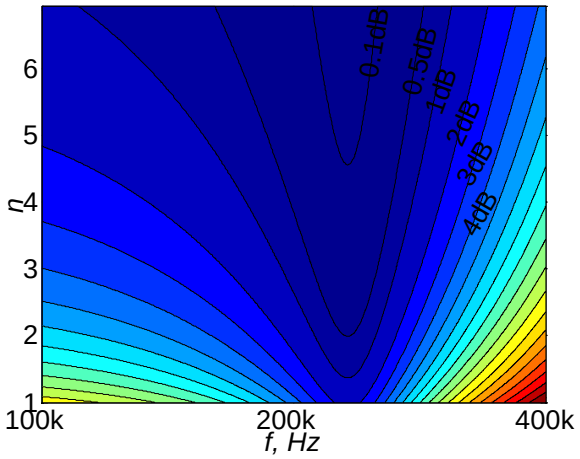

Figure 7. NF vs. *f* and *n* for high Z_s transducer used with FET amplifier

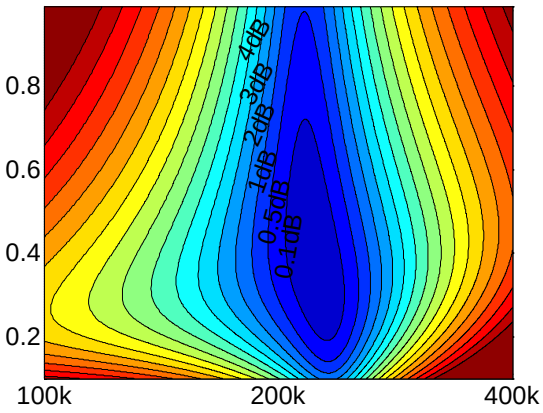

Figure 8. NF vs. *f* and *n* for high Z_s transducer used with BJT amplifier

It should be noted here that transformation coefficient *n* for BJT amplifier is lower than 1, e.g. the step-down transformer should be used.

4. Experimental investigation

The obtained theoretical results have been investigated experimentally. The noise figure measurement for signal source with complex output impedance is complicated. Therefore the signal, noise and SNR improvement have been measured in experimental verification.

4.1. The system

The system for signal propagation and absolute noise level measurement over the frequency range has been developed. The programmable DDS generator is used for the transmitting transducer excitation. The variable gain amplifier and A/D converter are used for data acquisition. The tested preamplifier is inserted immediately after the receiving transducer.

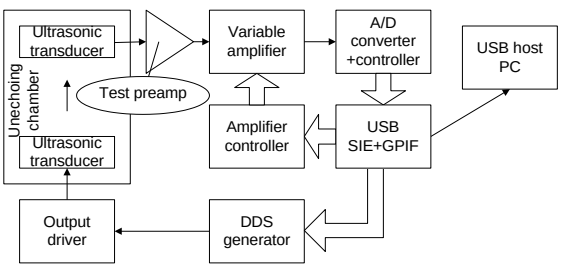

Figure 9. Measurement system

Data is collected and all the processing accomplished in host PC, connected via USB 2 interface.

4.2. Noise measurement

Noise measurement is done by taking the FFT of the signal at the tested preamp output (no excitation).

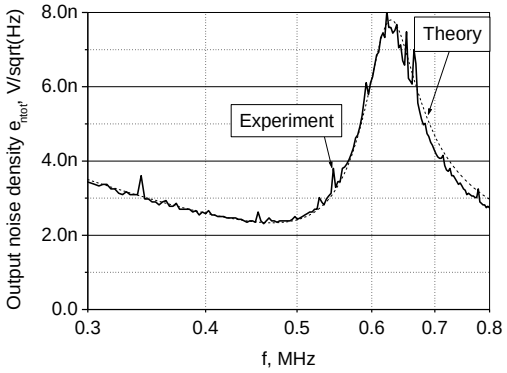

Figure 10. Measured vs. theory noise

Results in Figure 10 present noise spectral density at preamp input. The theory values are calculated using equation (5) divided by equation (4).

Same way the results for the transformer matching investigation have been obtained. Other type, air-coupled ultrasonic transducers have been used for next investigation. Same operational amplifiers have been used. Figure 11 is representing the results for experimentally obtained noise spectral density. Figure 12 is for measured signal spectral density. Figure 13 is for calculated SNR improvement when transformer matching is applied.

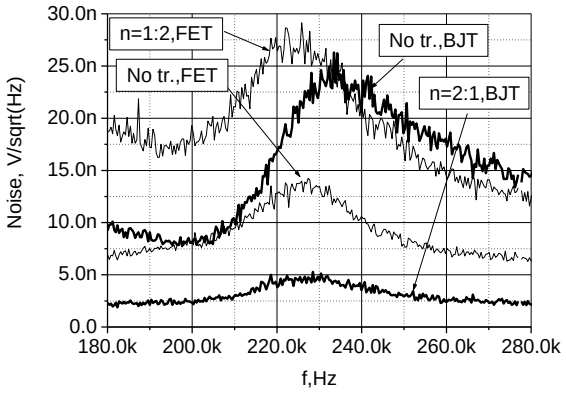

Figure 11. Measured noise

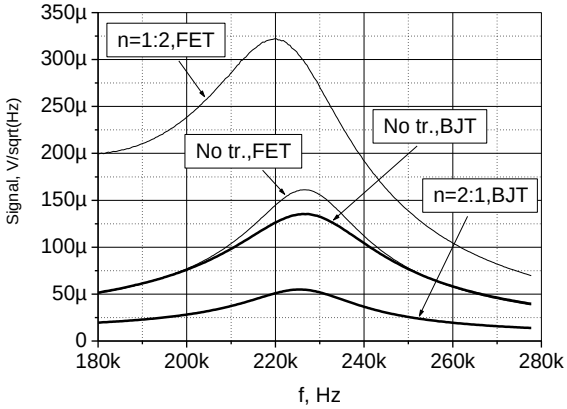

Figure 12. Measured signal

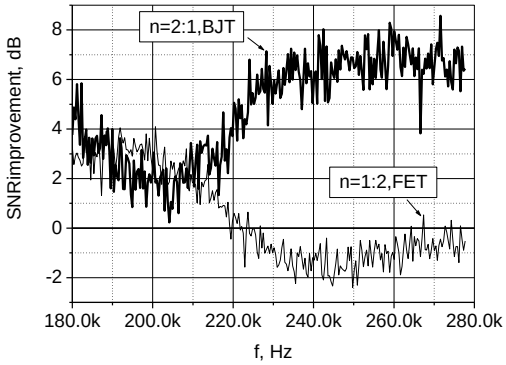

Figure 13. SNR improvement

5. Conclusions

The theoretical and experimental investigation confirmed the ability to improve the ultrasonic preamplifier noise performance basing the theoretical analysis. In the particular application analysed transformer application allows for 7dB SNR improvement. The improvement is confirmed using the measurement system described.

References

[1] P.A.Lewin, "Quo vadis medical ultrasound?", Ultrasonics, 42, 2004, pp.1–7.

[2] M.C.Wijk, J.M.Thijssen, "Performance testing of medical ultrasound equipment: fundamental vs. harmonic mode", Ultrasonics, 40, 2002, pp.585–591.

[3] L. Svilainis V. Dumbrava, "Design of a low noise preamplifier for ultrasonic transducer", Ultragarsas, 55, Technologija, Kaunas, 2005, pp.28-32.

[4] C.D.Motchenbacher, J.A.Connelly, Low noise electronic system design, John Willey & Sons Inc., 1993.

[5] T. L. Rhyne, "Characterizing Ultrasonic Transducers Using Radiation Efficiency and Reception Noise Figure", IEEE trans. UFFC, 45, 1998, pp.559- 566.

[6] W.M.Leach, "Noise analysis of transformer-coupled preamplifiers", J.Audio Eng. Soc., 40, 1992, pp. 3-11.

[7] Ch.Trask, "Designing wide-band Transformers for HF and VHF Power Amplifiers", QEX/Communications Quarterly,2, 2005, pp. 3-15.

[8] V.Dumbrava, L.Svilainis, "Application of transformer for improvement of noise performance of ultrasonic preamplifier", Ultragarsas, 57, Kaunas, 2005, pp.22-28.

[9] S.Sherrity et.all., "Accurate equivalent circuit for the unloaded piezoelectric vibrator in the thickness mode", J. Phys.D: Appl. Phys., 30, 1997, pp. 2354–2363.

[10] L.Svilainis V.Dumbrava, "Investigation of a preamplifier noise in a pulse-echo mode", Ultragarsas, 56, Kaunas, 2005, pp. 26-29.

A COMPUTER-AIDED DETECTION AND DIAGNOSIS FOR MICROCALCIFICATIONS IN DIGITAL MAMMOGRAMS

Song Lixin, Gao jie, Zhang kaiyu, Shi Shengjun

Harbin university of science and technology
Harbin 150080, P. R. China
T.86-451-86396216; F. 86-451-86396201; E.lixins99@yahoo.com.cn.

Abstract

To the question that the microcalcifications (MCCs) in the mammography are extremely small, various shapes, different size, variable distributions, and low contrast. The intensity difference between suspicious areas and their surrounding tissues can be quite slim. According to the principle that microcalcificatins are relatively high-frequency components buried in the background of low-frequency components and very high-frequency noise in the mammograms, the paper presents a method to detection the microcalcifications by morphology and wavelet transform. And according to the principle that artificial neural network can implement classification through training, the paper presents a method to identificate the types of pathological changes by probability neural network (PNN). Experiments indicate that the algorithm not only has simple operation, and achieves high true positive detection rate(TPR) at the cost of low false positive(FP).

1. Introduction

Breast cancer is the second cause of death among women cancers. There is one person die of breast cancer each 13 minutes. There is clear evidence which shows that early diagnosis and treatment of breast cancer can significantly increase the chance of survival for patients. Since the cause of breast cancer is still unknown, the earlier the cancer is detected, the better the chance that a proper treatment can be prescribed.

Detection methods are based on clinical examination, mammography, ultrasound, and core biopsy. Of these methods, mammography is the only reliable and practical method capable of detecting breast cancer at its early stage. Between 30%~50% of all breast malignancy exhibit microcalcifications, and the key technology of early diagnosis of breast cancer is to find the MCC in the mammography and estimate the tendency of malign. MCCs normally have a higher X-ray attenuation than the normal breast tissue and appear as a group of small localized granular bright structures in the mammograms. Two typical mammograms with MCC clusters are shown in Figure 1(a), (b) and the ROIs include suspicious MCC are shown in Figure 1(c), (d).

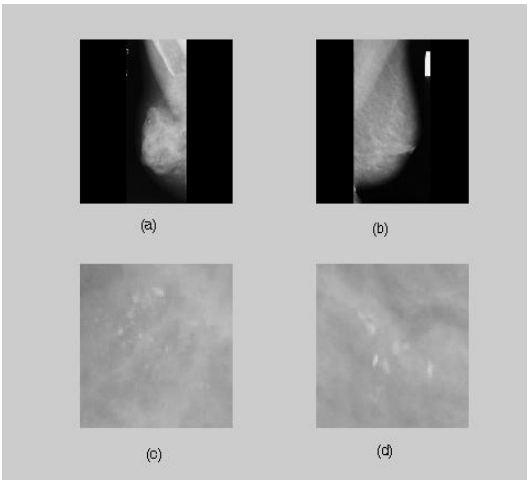

Figure 1. (a), (b) Typical mammograms with MCCs. (c), (d) ROIs which include MCCs

At present, the main methods of detecting MCCs include tradition image processing technology, wavelet transform, morphology, an artificial neural network etc. and the combining of several methods[1][2][3][4][5]. The single method above has higher TPR, but at the same time has higher FP.

This paper presents a computer-aided detection for clustered MCCs and classification the region of interest (ROI) into benign or malignant. The method proposed first extracts the suspicious MCC area (ROI) from the image using the (x, y) coordinates and radius value already provided by radiologist in the database MIAS. Our method has two separate steps. In the first step, we use morphological approach to isolate the breast background from the MCCs and gain a bilevel image I_m (x,y), and use wavelet transform to detection the MCCs and also gain a bilevel image I_w (x, y), then make a logical and operation I_m (x, y) and I_w (x, y) to realize the detection of MCCs. In the second step, an artificial neural network PNN is used to estimate the likelihood of malignancy or benign using the extracted features as input.

2. Microcalcification Detection

MCCs appear as tiny, circular deposits of calcium, which can vary in size from 0.1mm~1mm and usually marginally brighter than the background. From an image processing point of view, MCCs are relatively high-frequency components buried in the background of low-frequency components and very high-frequency noise in the mammograms. So, in the first step, the aim is to delete the low-frequency and very high-frequency components and realize the detection of MCCs. We use the top-hat transform of morphological approach to separate the MCCs from the background and use the wavelet transform to delete a part of the low-frequency and very high-frequency signal, and then utilize the logical and operation to gain the location of MCCs.

2.1. Morphological

MCCs appear on the mammography as circular bright spots, and a calcification has approximately a size of 20 pixels on each mammogram[2], so we chose a structuring element larger than 20 pixels. And they have low contrast. The properties of MCCs enable them to be detected through morphological approach.

Let $f(x, y)$ be an image and g be a structuring element. Then the elementary operation Erosion and Dilation are defined as follows (1-D):

$$f \Theta g = \wedge\{f_{-x} - g(x) : x \in D[g]\} \quad (1)$$

$$f \oplus g = \vee\{f_x + g(x) : x \in D[g]\} \quad (2)$$

Where $\wedge$ and $\vee$ are defined as follows:

$$(f \wedge g)(x) = \min\{f(x), g(x)\} \quad (3)$$

$$(f \vee g)(x) = \max\{f(x), g(x)\} \quad (4)$$

By combining erosion and dilation, the important morphological filter operations opening and closing are formed:

$$f \circ g = (f \Theta g) \oplus g \quad (5)$$

$$f \bullet g = -[(-f) \circ (-g)] \quad (6)$$

A gray value image is imagined to be a 2-D surface in 3-D space. An opening operation to the ROI keep the breast background and this means the positive peaks in the gray-value surface smaller than the structuring element are removed, and the structuring element chose is a little larger than the maximal size of MCC. Therefore the impossible MCCs are removed by opening operation. So we subtract this background from the original image to recover the positive peaks:

$$HAT(f) = f - (f \circ g) \quad (7)$$

Then we threshold the result image $HAT(f)$ using the value of 3.4σ, σ is the standard deviation of the result image.

Figure 2 shows the processing result using morphological.

2.2. Wavelet Transform

Since wavelets are localized in both the space and frequency domains, they have a multiresolution property. This makes it suitable for extracting MCCs from low-frequency backgrounds and high-frequency noise [6]. In particular, the wavelet transform decomposes the signal into signal bands of different frequency ranges. It can help to identify useful information relevant to MCCs and discard the signal bands which make little contribution to detection.

(a) (b) (c)

Figure 2. The ROI and the detection result using morphological. (a) ROI. (b) The image after Top-Hat operation. (c) The image after global thresholding

The wavelet used in this study is Daubechies orthogonal wavelet of length four. The ROIs are decomposed up to four levels using the wavelet transform. The 2-D scaling and wavelet function are defined as follow:

$$\phi(x,y) = \phi(x)\phi(y) \quad (8)$$

$$\psi^1(x,y) = \psi(x)\psi(y) \quad (9)$$

$$\psi^2(x,y) = \psi(x)\phi(y) \quad (10)$$

$$\psi^3(x,y) = \phi(x)\psi(y) \quad (11)$$

Where $\phi(x)$ and $\psi(x)$ are 1-D wavelet and scaling function.

Let $f(x,y)$ be an gray image, and it can be decomposed by the wavelet transform as follows:

$$A_j(m,n) = < f(x,y), \phi_{j,m,n}(x,y) > \quad (12)$$

$$D_j^1(m,n) = < f(x,y), \psi_{j,m,n}^1(x,y) > \quad (13)$$

$$D_j^2(m,n) = < f(x,y), \psi_{j,m,n}^2(x,y) > \quad (14)$$

$$D_j^3(m,n) = < f(x,y), \psi_{j,m,n}^3(x,y) > \quad (15)$$

Here, A is low frequency components; D^1, D^2, D^3 are horizontal, vertical and diagonal high-frequency components.

We generalized the wavelet decomposition by multiplying certain weighting value at each level *j* to enhance MCCs as well as suppressing background structures and noise. The reconstruction image $f'(x,y)$ is given by:

$$f'(x,y) = \alpha A_L(m,n) + \beta \sum_{j=2}^{L} (D_j^1(m,n) + D_j^2(m,n) + D_j^3(m,n)) + \chi(D_1^1(m,n) + D_1^2(m,n) + D_1^3(m,n)) \quad (16)$$

The wavelet used in this study is Daubechies orthogonal wavelet of length four. The ROIs are decomposed up to four levels using the wavelet transform. We chose to do the reconstruction by weakening LL_4 (corresponding the low-frequency background) and HL_1, LH_1, HH_1 (corresponding the very high-frequency noise) and enhancing $HL_{2,3}$, $LH_{2,3}$, $HH_{2,3}$. The reconstruction image is shown in Figure 3(a). And then using global threshold gain the location of MCCs. The bilevel image is shown in Figure 3(b).

2.3. Logic AND operation

In order to realize the detection of MCCs, we use logical AND operation to utilize the advantage of morphological approach and wavelet transform

$$I_r(x, y) = I_m(x, y) \text{ AND } I_w(x, y) \quad (17)$$

Eventually we realize the detection of MCCs. The result of logical AND operation is shown in Figure 3(c).

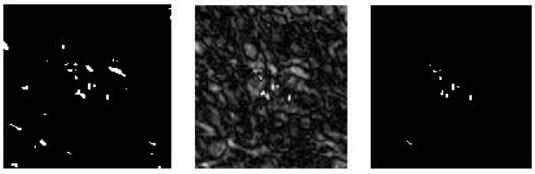

(a) (b) (c)

Figure 3. Detection result using wavelet and logical AND. (a) The reconstruction image $I_{w0}(x, y)$. (b) The bilevel image after global threshold $I_w(x,y)$. (c) The location of MCCs $I_r(x,y)$

3. Classify ROIs into Malignant or Benign

We extract features from the ROI and the bilevel image $I_r(x,y)$ separately, then utilize PNN to classify the ROIs into malignant or benign. The feature set is consisted of eight features. They are the pixel intensity variance (var), the energy variance (evar), the average (avg), the average-energy (eavg), the skewness (skew), and the kurtosis (kurt) from the original ROI, and the number of MCCs (num), the Euler number (eul) from the bilevel image.

We have selected PNN for classification purpose, which has 2 layers. When an input is presented, the first layer computes distances from the input vector to the training input vectors, and produces a vector whose elements indicate how close the input is to a training input. The second layer sums these contributions for each class of inputs to produce as its net output a vector of probabilities. Finally, a compete transfer function on the output of the second layer picks the maximum of these probabilities, and produces a 1 for that class and a 0 for the other classes.

Our method was evaluated with 50 ROI images (64×64 pixels) including 14 benign ROIs, 15 malignant ROIs and 21 ROI without MCCs. We use 35 ROIs being randomly selected for the training, and the rest 15 ROIs for testing.

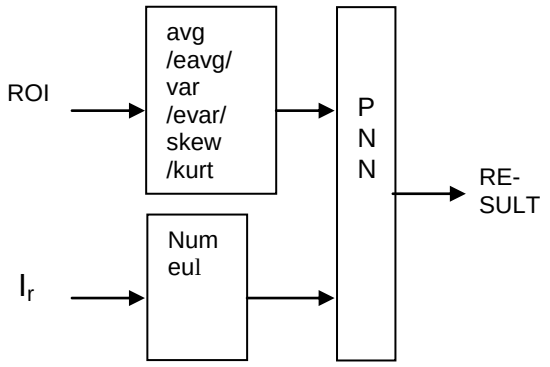

Figure 4. Mixed feature neual neural network for classifying the ROIs

4. Results and Discussions

The result of the detection of MCCs is shown in the Table 1. It achieves a 80.2% mean true positive detection rate at the cost of 2.45 false positive per ROI.

Table 1. The Results of Detection

ROI	The number of MCCs	Results	
		TPR	FP
Total	294	236/294(80.2%)	2.45

We utilize the PNN to classify the ROIs into malignant, benign and without MCCs. The recognition accuracy is 83.3% considering the malignant ROIs alone, 75% for the benign ROIs, and 60% for the ROIs without MCCs alone. The total accuracy is 73.3%. The results are expressed in terms of True Positive (TP). The results are shown in Table 2.

Table 2. Recognition score

	No. of ROIs	TPR	
		Training set	Test set
Malignant	15	8/9(88.9%)	5/6(83.3%)
Benign	14	10/10(100%)	3/4(75%)
without MCCs	21	14/16(93.8%)	3/5(60%)
Total	50	32/35(91.4%)	11/15(73.3%)

5. Conclusion

In this paper, we use wavelet transform and morphology to automatically detect MCCs in digitized mammograms. Use PNN Classify ROIs into Malignant or Benign. The proposed method is very efficient for automatically detect and Classify MCCs in mammograms. The conclusions are as follows: the combining of wavelet transform and morphology ensure higher TPR and reducing the FP.

References

[1] Noha Youssry, Fatma E.Z. Abou-Chadi and Alaa' M.El-Sayad. "Early detection of masses in digitized mammograms using texture features and neuro-fuzzy model", Proc. Of 4th International IEEE EMBS Special Topic Conference on Information Technology Applications in Biomedicine, 2003, pp. 226–229.

[2] Wan Mimi Diyana, Julie Larcher, and Rosli Besar. "A comparison of clustered microcalcifications automated detections in digital mammogram", Proc. Of ICASSP'03, 2, 2003, pp. 385-388.

[3] Wang T.C, Karayiannis N.B. "Detection of microcalcifications in digital mammograms using wavelets", IEEE Trans. Med. Imaging, 17(4), 1998, pp.498–509.

[4] H.D.Cheng, and Jingli Wang. "Fuzzy Logic and Scale Space Approach to Microcalcification Detection", Proc. Of ICASSP'03, 2, 2003, pp.345-348.

[5] Michael Wirth, Matteo Fraschini, Jennifer Lyon. "Contrast enhancement of microcalcifications in mammograms using morphological enhancement and non-flat structuring elements", Proceedings of the 17th IEEE Symposium on CBMS'04, 2004, pp.1063-7125.

[6] Songyang Yu, and Ling Guan. "A CAD System for the Automatic Detection of Clustered Microcalcifications in Digitized Mammogram Films", IEEE Trans. Med. Imag.,19(1), 2000, pp. 115-126.

CELP CODE BOOK WITH INDEX PREDICTION

Snejana Pleshkova – Bekiarska, Damian Damianov

Technical University – Sofia, Bulgaria
snegpl@tu-sofia.bg ellov@abv.bg

Abstract

The code book is one of important blocks in the CELP speech coding method, with which it is possible to make the vector quantization (VQ) of each speech sub frame. This reduces the speed of transmission replacing the sub frame with the index of most similar excitation vector in the stochastic CELP code book. In the decoder the received index is used as an address of the same stochastic code book as in the coder to produce the excitation vector, with which it is prepare the speech synthesis CELP algorithm.

In this article it is proposed an approach to reduce additionally the speed of CELP transmission with a method of index prediction. The proposed method is connected with minimal additional components in CELP speech coding and decoding and some little increasing of calculations. There are present the equations describing the proposed method. Some simulations are made for feature establishment of the proposed method and some of the results of these simulations are present in comparative style to reviewing the advantages of this method.

1. Introduction

In the CELP speech coding method there are two code books: stochastic and adaptive [1]. The adaptive code book work as a long term prediction filter for pitch prediction [2]. The stochastic code book prepare a vector quantization of speech signals. In this code book there is a collection of predefined and stored excitation vectors. The comparison of each of these vectors with the corresponding vectors of current subframe vector of the original speech signal give the decision that one of these vectors is more similar to the original speech signal subframe. The address or index to the place in the stochastic code book, where this vector is stored is transmitted after the coding of the current speech frame. This operation is called code book search, because the vector the vector is find after a procedure of mean square error calculating and minimization. The transmission of the code book index instead of situated in the code book excitation vector give a suitable bit rate reduction. But after that still redundancy in speech signal rest and it is possible to search some additional means or algorithm to improve the bit rate reduction. One such a method is proposed in this article – the method of code book indexes prediction. First it is given a brief presentation of the basic operation of the CELP coder with the place of the stochastic code book and the main equations describing the code book search procedure. Then it is present the proposed modification of this part of the CELP coder, where it is added the index prediction. The proposed modification is argued with the corresponding equations. At the end of the article there are presented the comparative results of simulations and testing of the proposed method with real speech signals coded and then decoded with a standard CELP system with and without of the proposed code book index prediction.

2. Basic CELP Operations

The code books are shown in Fig. 1.

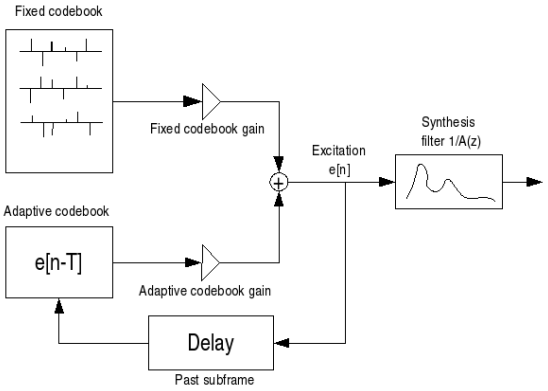

Figure 1. CELP code books

The stochastic code book is named "Fixed" because the content of the code book is constant and is preliminary filed with a lot of vectors (usually the number of vectors is 512). The "Adaptive code book" calculate the pitch T as a difference $e[n-T]$ between the current n and "Past subframe". The output vectors of the "Fixed" and "Adaptive" code books are multiplied with the corresponding gains "Fixed code book gain" and "Adaptive code book gain". These two parts are summing $\oplus$ and form of the excitation vector $e[n]$. The excitation vector $e[n]$ is then performed as the current synthesis speech subframe $\hat{s}(n)$ with the short term synthesis filter $1/A(z)$:

$$A(z) = 1 + \sum_{i=1}^{P} a_i z^{-i}, \qquad (1)$$

where

a_i are the coefficients of the speech frame analysis filter;

P – the order of the speech frame analysis filter (in CELP standard usually $P = 10$.

The procedure of code book search by means of iterative calculating and minimization of the mean square error is shown in Figure 2.

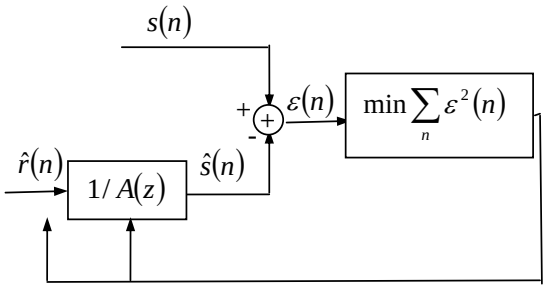

Figure 2. Code books search

The current subframe of the original speech signal $s(n)$ is compared (subtracted) with the current subframe of the synthesis speech $\hat{s}(n)$ build from the chosen excitation vector $e(n)$, as is shown in Figure 1. The result of this comparison is the error $\varepsilon(n)$:

$$\varepsilon(n) = s(n) - \hat{s}(n) \qquad (2)$$

The minimization of the mean square error:

$$\min \sum_{n} \varepsilon^2(n) \qquad (3)$$

is performed by choosing each time a new vector from the stochastic code book, calculating the error $\varepsilon(n)$ and then check the square error for the minimum. If these minimum is found, then the index of the corresponding vector in the stochastic code book is transmitted. It must to imply from the Figure 2, that the determined index is the output of the block, which prepare the error minimization $\min \sum_{n} \varepsilon^2(n)$. The sequence of the indexes follow the sequence of the subframes and is added to the rest of parameters transmitted for each frame of the analysed original speech frame. The quantity of the information transmitted for each index depend of the number of excitation vectors in the stochastic code book (usually the number of vectors is 512) and hence the number of bits transmitted for each index is 9. To reduce this quantity of

transmitted information it is proposed in this article to perform an index prediction before of their transmission.

3. Stochastic Code Book Index Prediction

The place, where it is possible to add the stochastic code book index prediction is shown in Figure 3.

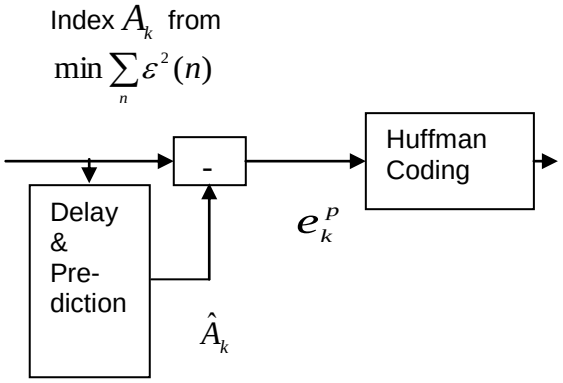

Figure 3. Stochastic code book index prediction

The input for the prediction in Figure 3 is the sequence of the indexes A_k, which is the output of the block of minimization $\min \sum_n \varepsilon^2(n)$ in Figure 2. To perform the prediction it is necessary to story some of the past values of the indexes A_k. This is done with the block named Delay & Prediction. Also in this block the stored past values are used for calculating the predicted value $\hat{A}_k$ of the current index A_k:

$$\hat{A}_k = \sum_{i=1}^{N} a_i A_{k-i} \ , \qquad (4)$$

where

N is the order of the prediction and can be chosen experimentally by controlling the decreasing of the quality of the decoded speech signals:

a_{i} – the coefficients of the prediction filter.

The substraction of the current index A_k and the predicted value $\hat{A}_k$ give the error e_k^p:

$$e_k^p = A_k - \hat{A}_k \qquad (5)$$

It is known from the prediction theory [3] that the variances of the prediction error e_k^p are in principles more less than the variances of the indexes A_k. Then it is evident that the transmission of the prediction error e_k^p instead of the indexes A_k can be made with less number of bits, than the transmission of indexes A_k.

To gain an additional reduction of the bit rate transmission it is proposed on the Figure 3 to use Huffman coding [4] after the stochastic code book index prediction. It is known, that Huffman code is an irregular method of coding and it is necessary to examine and define the length of the Huffman code. This is possible if there is a representative statistic of variances of stochastic code book indexes A_k and respectively of the prediction error e_k^p.

4. The Code Book Index Characteristics Analysis

The effect of the proposed method of stochastic code book index prediction can be increased if the positions of the excitation vectors placed in stochastic code book are chosen in a manner, that their correlation give the minimal variances in prediction error e_k^p. That means the values of indexes for the neighbouring subframes, chosen after minimization of the mean square error can be also neighbouring if it is possible. This condition can be prove be means of the equation for disordering of vectors in the stochastic code book:

$$D_\rho = W_\rho \sum_{i=1}^{S} \sum_{j=1}^{S} \rho^{|i-j|} d(y_i, y_j), \qquad (6)$$

where

$d(y_i, y_j)$ is Euclidean distance between $i-th$ and $j-th$ code vectors;

$\rho \in [0,1]$ – coefficient to improve the weight of vectors, which are very close in the code book.

There are some possibilities to decrease the disordering of vectors in the stochastic code book. For example: the Kohonen Neural Network [5] or other self organized Neural Networks [6], but it is the object of the future work.

5. Results of Experiments and Conclusion

Some experiments are prepared for testing the properties of the proposed method of stochastic code book index prediction. For the test are used simulated and real speech signals, which are coded and then decoded using both the standard CELP method and proposed method with stochastic code book index prediction. The generalized results as a comparative presentation of calculated segmental signal to noise ratio (SEGSNR) are present in the Table 1. These results shows that for simulated sinusoidal signals (Sin600Hz and Sin1600Hz) and real (Female and Male) speech signals there are little degradations of segmental signal to noise ratio (SEGSNR) for the proposed method with stochastic code book index prediction. It can be supposed, that this is because the order of prediction is not enough, but it is chosen small to keep the calculations little. Also it is possible to improve the segmental signal to noise ratio (SEGSNR) for the proposed method with stochastic code book index prediction if it is performed one of the above mentioned for decreasing the disorder of vectors in the stochastic code book.

Table 1

Test signals	SEGSNR for standard CELP method	SEGSNR for index prediction method
Sin600Hz	9,3452	10,0654
Sin1600Hz	10,6734	9,6453
Female	8,6733	8,6689
Male	7,8567	7,6590

References

[1] Kondoz, A.M. Digital speech coding for low bit rate communication systems. Yohn Wiley&Sons, New York, 2000.

[2] Federal Standard 1016, "Telecommunications: Analog to digital conversion of radio voice by 4800 bit/second code excited linear prediction (CELP)", National Communication System-Office of Technology and Standards, Feb. 1991.

[3] Atal B.S. and Remde J.R., A new model of LPC excitation for producing natural-sounding speech at low bit rates. Proc. IEEE-ICASSP, Paris, France, 614-617, 1982.

[4] Cormen Thomas H., Charles E. Leiserson, Ronald L. Rivest, and Clifford Stein. Introduction to Algorithms, Second Edition. MIT Press and McGraw-Hill, 2001. ISBN 0-262-03293-7. Section 16.3, pp.385–392.

[5] Kohonen T., Self – Organization and Associative Memory, 2nd Edition, Springer – Verlag, 1988.

[6] Riskin E.A., Atlas L.E., Lay S.R., Ordered neural maps and their applications to data compression, Proc. IEEE Workshop on Neural Networks for Signal Processing, pp.543-551, September 1991.

DEVELOPMENT OF A SERIAL INTERFACE FOR TV MONITORS ADJUSTMENT WITH COMPUTER

Alexander Bekiarski, Andrei Andreev

Technical University – Sofia, Bulgaria
aabbv@tu-sofia.bg aandreev@tu-sofia.bg

Abstract

The modern TV monitors and TV receivers are made with possibilities to automatically adjustment of there parameters, for example horizontal and vertical frequencies in dependence from the input horizontal and vertical synchronization pulses. This is done with implementation of programmable integrated circuits, using a build in the monitor or receiver microcomputer and a memory for these values.

It is very interesting to have the possibilities to control this process of adjustment, made this manually and do the appropriates measurements of the defined horizontal and vertical frequencies, when the monitor or receiver can be repaired or tested. Of course, it is possible to combine these measurements with some visual observations of displayed testing signals and data on the monitor screen of the computer. All that can be made with the proposed tool, which is connected to a computer with a serial interface.

1. Introduction

The modern CRT and Flat TV monitors and TV receivers are controlled by the embedded microcomputers. This is the common way to free the users from unusual and some time “unclear” adjustments, which are necessary to prepare. At the time of manufacturing the necessary parameters of each TV monitor or receiver are stored in the memory connected to the embedded microcomputer. When TV monitor or receiver are switched on the current setting parameters are transmitted from the microcomputer to control registers of the programmable integrated circuits. This procedure is sufficient for the normal operation of TV monitor or receiver. But at the time of repairing TV monitors or receivers there is the need some time to update all or to change some of the parameters stored in the memory. For making this operation it is necessary to have the possibility to input values of these parameters and changing it dynamically. This can be done if there is a special interface between the TV monitor or receiver and a desktop computer. Therefore the goal of this article is to propose a minimal additional hardware and software to connect the desktop computer and TV monitor or receiver, using both the standard desktop computer interfaces and the standard I2C characteristics.

2. The Block Schema of the proposed Serial Interface

The block schema is shown in Fig. 1.

Desktop computer have some standard interfaces like Parallel, Serial, USB etc. [1]. From the characteristics of the I2C standard it is know [2], that the speed of the I2C interface used in the TV monitors or TV receivers is not so high. The Standard – mode data transfers can be made at up to 100 kbit/s, which is sufficient for the transferring of data for/to Desktop Computer and TV monitor or TV receiver. Here it is chosen to use the Standard – mode I2C data transfer and this give the reason to

choose as a standard desktop interface - the Serial RS 232 Interface [3]. As it is shown in Figure 1, when this choice is made, it is necessary to design a special hardware part, named RS-232 to I2C Converter to resolve the differences between the to types of interfaces.

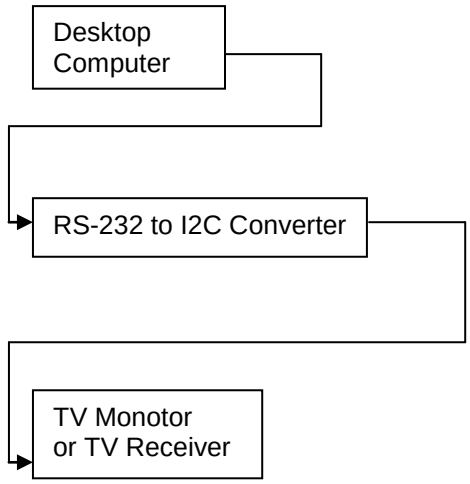

Figure 1. Block schema of the proposed serial interface

3. RS-232 to I2C Converter

The schema of proposed RS-232 to I2C Converter is shown in Figure 2.

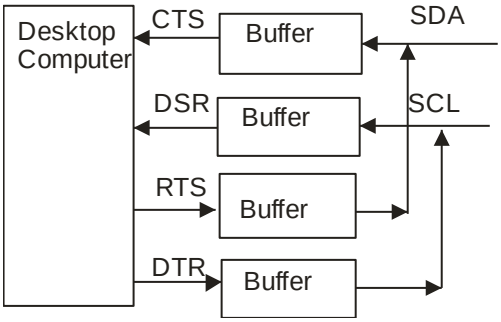

Figure 2. The schema of the proposed RS-232 to I2C Converter

In principle, the standard serial interface is designed to transfer serial data between the desktop computer and other devices equipped with this interface. The signals and protocol for data transferring via this interface are described in details in Standard RS-232, but it is possible to imagine, to take the control over the each of these signals and to produce the signals equivalents and corresponding to the standard I2C signals. This is the main idea of the proposed RS-232 to I2C Converter shown in Figure 2. In the RS-232 standard there are some modifications related to the number of pins of the used connectors, for example 9 – pin connector or 25- pin connector. Some of them, TXD - Transmit Data and RXD–Receive Data, are related directly to the data transmission, other are named control signals, for example RTS - Request to Send, CTS - Clear to Send, DSR - Data Set Ready, DTR - Data Terminal Ready etc. are control signals, driven the right data transfer. It is more convenient to choose these control signals for proposed RS-232 to I2C Converter. On the Figure 2 it is shown, that the desktop computer part of the converter use four signals CTS, DSR, RTS and DTR. On the other hand, the I2C part of the proposed converter use only two signals SDA and SCL. To resolve this differentce there are placed the blocks named "Buffer" and the arrow directions give the idea how the transfer is arrange.

7. Conclusion

The proposed serial interface for TV monitors and receivers is described briefly, but it is realized as a hardware module and it is made an user friendly software as a Windows Application in Visual C++ 6.0. The tests with designed serial interface for TV monitors and receivers adjustment are given the good results for the range of application – the professional dynamically adjustment or changing the programmable TV monitors and receivers parameters.

References

[1] Lazar Jonathan. Designing Computer Interfaces for Diverse User Populations. Yohn Wiley&Sons, New York, 2006.

[2] The I2C-Bus Specifications. Version 2.1, Philips Semiconductors, January 2000.

[3] Application Note 83. Fundamentals ofRS-232 Serial Communications. Dallas Semiconductors, September 1998.

FMNSWEBDOC – WEB BASED SYSTEM FOR DOCUMENTATION

A. Stoilov and V. Hristov

South-West University "Neofit Rilski"
Blagoevgrad, Bulgaria
Ivan Mihailov str. 66
E-mail: antonstoilov@abv.bg

Abstract

The system for documents exchange in one faculty is one of the most important part of program support of them. The purpose of paper is to present one possibility for using PHP, MySQL and Apache for realization of this system. The present web based system is applicable for different faculty. The real application of this product is present and running in web. The security system was developed.

1. Introduction

The FMNSwebDoc is an attempt to make web based systems for document storage. The instruments used for this realization are PHP and MySQL. This system is orientated in UNIX based servers such as Apache.

Documents are the basic building blocks of FMNSwebDoc. The software has possibility of doing the instance of documents from basic templates. All processes are done in Internet.

Other very important parts are the users. Each user has their own login name and password. Users can only alter items that they own, or that they administer. This means that individual users cannot make changes to other users' items. There are two special types of users:

- Users can be made into administrators (also known as 'superusers'). This overrides the normal access controls; an administrator can alter or edit anything.
- Restrict users are the persons how use this software only in his work.

Most projects or tasks have a group of users working together in one specific area. A usergroup is a group of users who share a similar work area. Notification emails can be sent to the usergroup, rather than just an individual user. This is available now and usergroups respond to the departments in faculty.

FMNSwebDoc has been developed on Red Hat Linux 9.0, Fedora'2006 and Debian (stable/testing) and run in a production environment with initially, PostgreSQL, and later MySQL databases. FMNSwebDoc will only run on PHP 4.2.0, or higher [1-4]. Earlier versions of PHP do not support $_POST, $_GET or $_REQUEST global arrays, which are necessary for FMNSwebDoc to function. The setup program of the system check for early versions of PHP and will record an error.

2. Basic conditions

With a web server such as Apache and MySQL, you have most of what you need to develop a web database application. The key glue you need is a way for the web server to talk to the database; in other words, a way to incorporate database operations into web pages. The most popular glue that accomplishes this task is PHP.

PHP is an open source project of the Apache Software Foundation and it's the most popular Apache web ser-

ver add-on module, with around 53% of the Apache HTTP servers having PHP capabilities [1-3]. PHP is particularly suited to web database applications because of its integration tools for the Web and database environments. In particular, the flexibility of embedding scripts in HTML pages permits easy integration of HTML presentation and code. The database tier integration support is also excellent, with more than 15 libraries available to interact with almost all popular database servers. Apache, MySQL, and PHP can run on a wide variety of operating systems.

PHP is a simple yet powerful language designed for creating HTML content. PHP runs on all major operating systems, from Unix variants including Linux, FreeBSD, and Solaris to such diverse platforms as Windows and Mac OS X. It can be used with all leading web servers, including Apache, Microsoft IIS, and the Netscape/iPlanet servers.

The language is very flexible. For example, you aren't limited to outputting just HTML or other text files – any document format can be generated. PHP has built-in support for generating PDF files, GIF, JPG, and PNG images, and Flash movies.

One of PHP's most significant features is its wide-ranging support for databases. PHP supports all major databases (including MySQL, PostgreSQL, Oracle, Sybase, and ODBC-compliant databases), and even many obscure ones. With PHP, creating web pages with dynamic content from a database is remarkably simple.

Finally, PHP provides a library of PHP code to perform common tasks, such as database abstraction, error handling, and so on, with the PHP Extension and Application Repository (PEAR). PEAR is a framework and distribution system for reusable PHP components.

The conception of development of FMNSwebDoc is present in fig.1. There is present three tiers corresponding with three level of communication. The first level is communication between client and server. The requests are available by Internet. Next level of transfer of requests is reports from database.

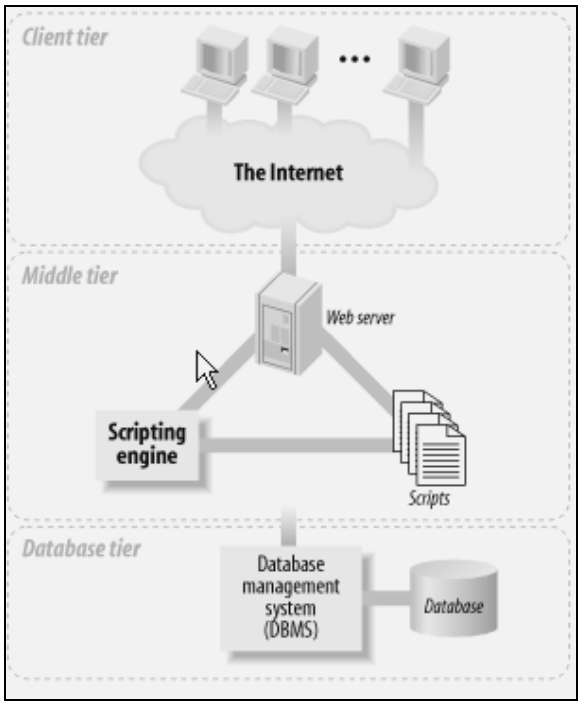

Fig. 1. Schematic of transfer of requests in FMNSwebDoc

The main advantages of this structure are: high security level, speed, separate of task and optimization of requisite hardware devices.

Most of the services we enjoy on the Web are provided by web database applications. Web-based email, online shopping, forums and bulletin boards, corporate web sites, and sports and news portals are all database-driven. To build a modern web site, you need to develop a database application.

The original FMNSwebDoc code was specifically written for a PostgreSQL database. The code now has a database abstraction layer and runs either MySQL or PostgreSQL. A calendar section and setup programs have been

added. Documentation for the program has been written. Work has also been done to enable FMNSwebDoc to work with Unicode (UTF-8) and other multibyte encoding systems. This is offered as an optional alternative, since MySQL prior to version 4.1 and PHP prior to version 4.3.0 have poor multibyte support.

The database types in the config file are:

- Postgresql => PostgreSQL abstraction layer.
- Mysql => standard MySQL abstraction layer
- Mysql_innodb => MySQL abstraction layer with innodb transaction support

In setup the administrator have possibility to choice on of them.

PostgreSQL is an Object-Relational Database Management System (ORDBMS) that has been developed in various forms since 1977. It began as a project named Ingres at the University of California at Berkeley. Ingres itself was later developed commercially by Relational Technologies/Ingres Corporation. In 1986 another team led by Michael Stonebraker from Berkeley continued the development of the Ingres code to create an object-relational database system called Postgres. In 1996, due to a new open source effort and the enhanced functionality of the software, Postgres was renamed to PostgreSQL, after a brief stint as Postgres95 [4]. The PostgreSQL project is still under very active development worldwide from a team of open source developers and contributors. PostgreSQL is an open source project. Open source by definition means that you can obtain the source code, use the program, and modify it freely without the confines of proprietary software. In the database world, open source means that you have honest access to benchmarking numbers and performance statistics, which companies such as Oracle prohibit. Open source, also means, that you are free to modify PostgreSQL to fit your particular needs.

The database used transactions. The PostgreSQL abstraction layer always uses transactions because:

- They provide better data security in the event of power failure or hardware/software crashes during database write operations. Incomplete data is not witten to the database, and data corruption or loss is avoided.
- Without transactions it is possible for two users to alter the same data simultaneously, leading to data corruption. With transactions this is prevented by design.

The mysql_innodb abstraction layer also uses transactions. For MySQL version 4.0, and above, innodb database support is enabled by default. For these versions (and configured 3.23.xx versions) it is recommended that the database be created with the mysql_innodb database creation script, and the mysql_innodb abstraction layer is used. For MySQL version 3.23.xx the database server must first be correctly configured to allow innodb databases to be used.

3. The web based system FMNSwebDoc

The scheme of the necessary tables in database is show in fig. 4. These tables are creating in case of choose MySql database. All tables are 14.

After creating of these tables is execute this two rows for initialization of "users" and "config" tables:

INSERT INTO users (id, name, fullname, password, email, admin, deleted)

VALUES (1, 'admin', 'Administrator', '0192023a7bbd73250516f069df18b500', 'please_edit@my_domain.com', 't', 'f');

INSERT INTO config (globalaccess, groupaccess, project_order, task_order) VALUES ('checked', '', 'ORDER BY name', 'ORDER BY name');

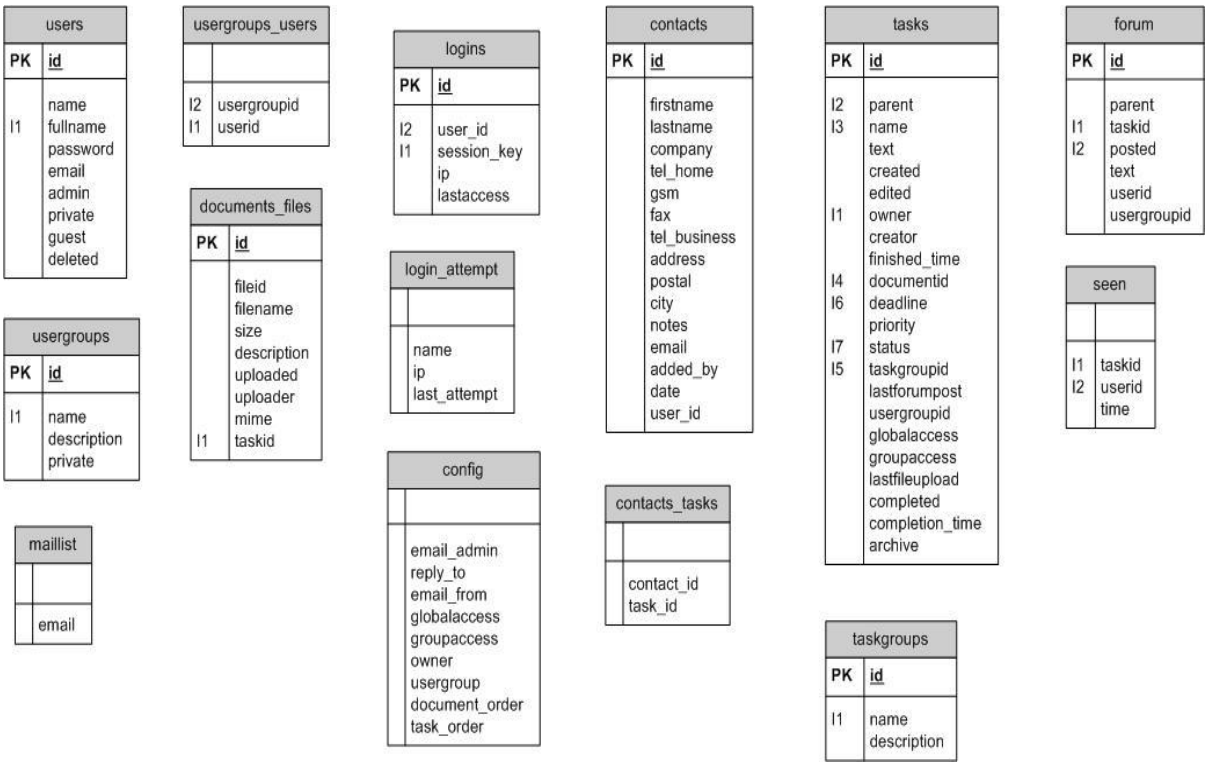

Fig. 2. Scheme of tables in database

Actualy, when finished the setup procedure we have one "super user": "admin" with password "admin123". With this account we create other accounts for each department. This data is remembered in "user" table.

For every department is created individual "usergroups", the data are in the same name table. We have and interstitial table – "usergroups_users". This table includes information for correspondence between user and usergroups, and for rapid recognition of usergroup of some user.

Every document generated by system, must by uploaded on the server. This procedure is manual, because the number of generated from templates documents in real is much more them the necessary and if all of these documents are uploaded automatically, the stability of system will be in danger. The information about these files is in "documents_files" table. The procedure for upload is shown in fig. 3.

Other very important tables are:

- "config" table – the table with value for main variables. This is initial values when system started
- "contacts" table – information for people in this work area.

We have and the table for forum. The form is place where every user have possibility to discussed with other users a theme how is important for all department.

When the program is started on the monitor is display the login. There is doing the check for user and privileges. In FMNSwebDoc are recognized two main accounts: administrator and user.

This process covered main aim of this system, namely creation of a catalogue for uploaded documents in one department.

Tasks are another part of documentation process in faculty. For this are create three tables:

- "tasks"
- "taskgroups"
- "contacts_tasks"

The names of tables are completing eloquent and the fields of these tables are present in fig. 2.

For assure the login was created two tables in database "login" and "login_attempt".

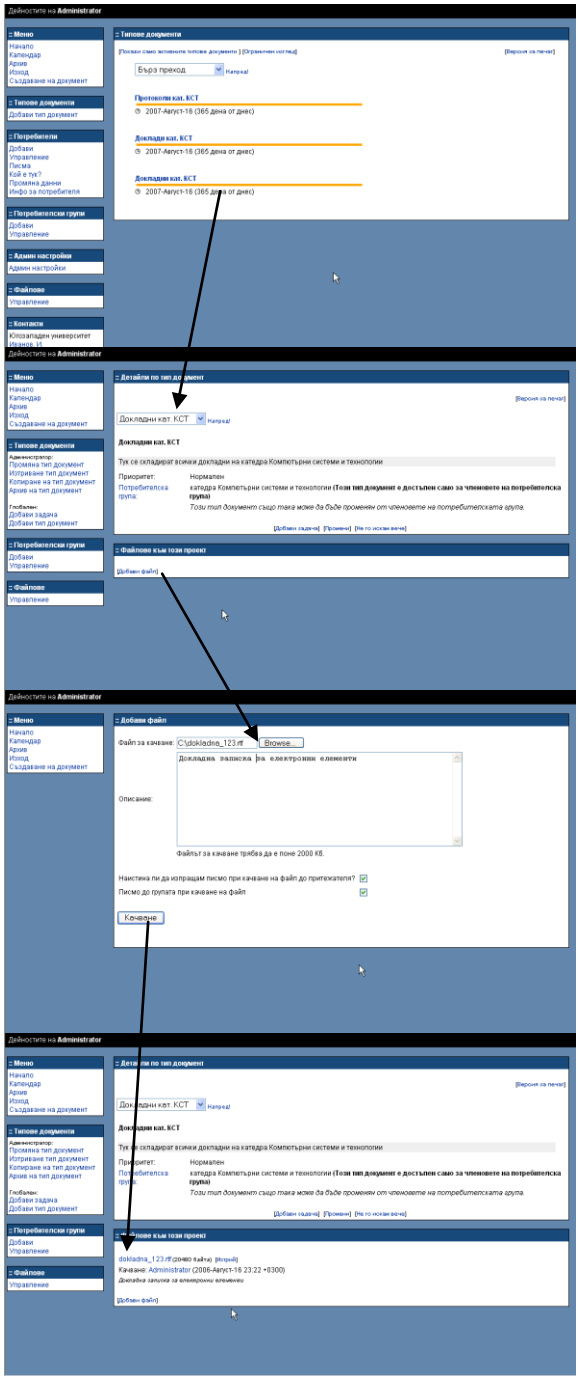

Fig. 3. The process for upload of filles

When is logged a user with administrative privileges it see the screen shown in fig. 4 and when is logged a user with users privileges it see the screen shown in fig. 5.

The user how is logged with users account was making:

- create the documents from templates;
- up-load of the instance documents;
- make archive from available documents;
- adding the new records in address book;

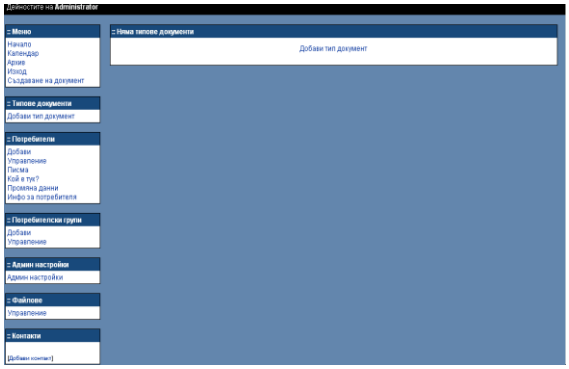

Fig. 4. Administrative start screen

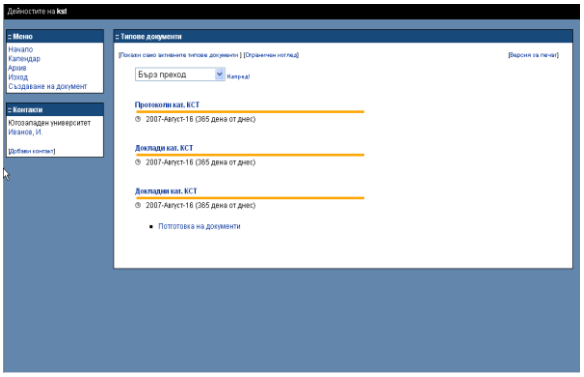

Fig. 5. Users start screen

The user how is logged with administrative account was making the same thinks like users plus:

- changes in administrative accounts;
- create new accounts;
- assignment of usergroups; corresponding with departments;
- e-mails settings;

- tracking of the activity of system;
- founding of banks for documents;
- definition of task for usergroups;

Realization of this aims was making with creations of the PHP scripts. The uploading documents are saving in database. The systems save documents with unique numbers. This numbers are two – one how is output number and second is input number. FMNSwebDoc has possibility for tracing the road of document and in the every moment is available at with office is situated. This possibility is available only for administrative accounts.

4. Security

FMNSwebDoc has been coded with strong security measures. In practical use FMNSwebDoc security has proven to be very robust. Practical measures to enhance security include:

- Shift the uploaded file directory to outside the web server root. FMNSwebDoc can write to anywhere in the file system. Check that the web server has write permissions for the chosen directory. This prevents uses uploading files, then navigating to the upload directory with a browser and executing the file.
- Shift the config file out of the webserver directories. You will need to alter the file [FMNSwebDoc]/path_config.php and add the new path to the include_path directive in php.ini.
- Shift the program files out of the webserver directories. You will need to alter the file [FMNSwebDoc] /path.php and add the new path to the include_path directive in php.ini.
- Use a non-root user for the database. The database users have minimal privileges, and not are able to create and/or delete tables.
- Make sure that Apache configuration allows .htaccess files to set <Limit> in FMNSwebDoc directory. FMN SwebDoc uses .htaccess files extensively to protect subdirectories.
- Make sure the file *[*FMNSwebDoc*] /config/config.php* is not world writable and not owned by the web server user.
- Use an SSL layer for access with FMNSwebDoc. Delete unnecessary files. For instance the *[*FMNSwebDoc*]/setup* directory and *[*FMNSwebDoc*]/update.php*. FMNSwebDoc is not tested nor supported on Microsoft IIS.

5. Conclusion

The present paper describes the developed web based system for documentation exchange in faculty. Based on analysis a decision was made for the operating system, web server, and dynamic pages platform is done. The functional diagram of the software and for the security design are proposed.

The real application of this product is present and running in web at address:

www.sec.swu.bg/pmf_doc/index.html.

References

[1] D. Sklar, Learning PHP 5, O'Reilly, 2004

[2] D. Sklar, A Trachtenberg, PHP Cookbook, O'Reilly, 2002

[3] R. Lerdorf, K. Tatroe, Programming PHP, O'Reilly, 2002

[4] P. DuBois, MySQL Cookbook, O'Reilly, 2002

[5] D. Dimitrov, Комуникационни системи в медицината, Изд. Технически Университет, София, 2005

ADVANTAGES AND DISADVANTAGES OF MAGNETOTHERAPY

Assoc. Prof. Jana Petrovska

M.D.Head Clinic Phys.Therapy and Rehabilitation University Hospital"St.Anna"
Sofia, Bulgaria

Summary

Electric currant with appropriate parameters can influence the patient's organism. Biological effect of Low frequency pulsating magnetic field(LPMF)is electrical effect-mainly anti-inflammatory, pain relieving and decongestant. The positive effect of LPMF is documented by studies.

Effects of changeless magnetic field is not electrical and is not documented by studies.

KEY WORD: magnetic field therapy, biological effect, changeless magnetic field, low frequency pulsating magnetic field.

AUTHOR INDEX